

# Interplay of Chiral Transitions in the Standard Model

Holger Gies,<sup>1,2,3,4,\*</sup> Richard Schmieden,<sup>1,†</sup> and Luca Zambelli<sup>5,‡</sup>

<sup>1</sup>*Theoretisch-Physikalisches Institut, Friedrich-Schiller-Universität Jena, D-07743 Jena, Germany*

<sup>2</sup>*Abbe Center of Photonics, Friedrich-Schiller-Universität Jena, D-07743 Jena, Germany*

<sup>3</sup>*Helmholtz-Institut Jena, Fröbelstieg 3, D-07743 Jena, Germany*

<sup>4</sup>*GSI Helmholtzzentrum für Schwerionenforschung, Planckstr. 1, D-64291 Darmstadt, Germany*

<sup>5</sup>*INFN-Sezione di Bologna, via Irnerio 46, I-40126 Bologna, Italy*

We investigate nonperturbative aspects of the interplay of chiral transitions in the standard model in the course of the renormalization flow. We focus on the chiral symmetry breaking mechanisms provided by the QCD and the electroweak sectors, the latter of which we model by a Higgs-top-bottom Yukawa theory. The interplay becomes quantitatively accessible by accounting for the fluctuation-induced mixing of the electroweak Higgs field with the mesonic composite fields of QCD. In fact, our approach uses dynamical bosonization and treats these scalar fields on the same footing. Varying the QCD scale relative to the Fermi scale we quantify the mutual impact of the symmetry-breaking mechanisms, specifically the departure from the second order quantum phase transition of the pure Yukawa sector in favor of a crossover upon the inclusion of the gauge interactions. This allows to discuss the “naturalness” of the standard model in terms of a pseudo-critical exponent which we determine as a function of the ratio of the QCD and the Fermi scale. We also estimate the minimum value of the  $W$  boson mass in absence of the Higgs mechanism.

## I. INTRODUCTION

In the standard model of particle physics, chiral symmetry breaking generates the masses of fermionic matter in the visible universe [1–3]. Two sectors of the standard model contribute apparently independently to fermion mass generation: at the Fermi scale, electroweak symmetry breaking triggered by the parameters of the Higgs potential induce current quark and charged lepton masses [2] through the Yukawa interactions to the Higgs field. Subsequently at the QCD scale, the intricate dynamics of the strong interactions generate the baryon masses that ultimately dominate the visible masses in the universe [4, 5]. With the Fermi scale corresponding to the vacuum expectation value of the Higgs field  $v \simeq 246$  GeV and the QCD scale  $\Lambda_{\text{QCD}} \simeq \mathcal{O}(100)$  MeV, the two relevant scales are 2-3 orders of magnitude apart.

The symmetry-breaking mechanisms are rather different in the two sectors: mass generation in QCD is driven by the gluonic interactions growing strong towards lower energies, thus being an intrinsically nonperturbative phenomenon. Mass generation in the electroweak sector – despite also being a gauge theory – is described by the Yukawa interactions with the Higgs field and appears accessible to perturbation theory. Also, all involved quantities including the two different scales given above can be traced back to different fundamental parameters of the model. Similar comments apply to typical embeddings of the standard model in overarching models, where the two scales are parametrized by the breaking mechanisms towards the standard-model symmetries.

The qualitative difference between the two mechanisms of chiral symmetry breaking becomes prominent when studying the symmetry transitions as a function of control parameters within reduced model sectors. For instance, reducing the electroweak sector to a pure Yukawa model involving the Higgs field and the most strongly coupled top and bottom quarks, the reduced model exhibits a chiral quantum phase transition of second order as a function of the mass parameter of the Higgs potential [6–8]. By contrast, the pure QCD sector is essentially governed by the strong coupling constant, and the long-range physics is always in the symmetry broken phase. The combination of the two sectors therefore suggests that the standard model is also always in the symmetry broken phase, but exhibits a rapid crossover as a function of a suitable control parameter.

This rapid crossover is also a manifestation of the so-called *naturalness problem* [9–13]: considering the standard model as a function of microscopic (bare) parameters at some high-energy scale  $\Lambda$  (an ultraviolet (UV) cutoff), one of its parameters serving as a control parameter has to be tuned rather finely to put the model rather close to the rapid crossover. This fine-tuning is necessary to separate the high scale  $\Lambda$  from the Fermi scale and the subsequent QCD scale,  $\Lambda \gg v > \Lambda_{\text{QCD}}$ . It should be emphasized that the naturalness problem is not a consistency problem of the standard model, but rather a peculiar feature that may or may not find an explanation within an embedding in a more fundamental theory.

The present work is devoted to a study of the interplay of the two chiral symmetry breaking sectors of the standard model. This interplay is visible in the details of how the two transitions merge into the expected rapid crossover. Moreover, it becomes apparent by the fact that the relevant degrees of freedom partly share the same quantum numbers: in the electroweak sector,

\* holger.gies@uni-jena.de

† richard.schmieden@uni-jena.de

‡ luca.zambelli@bo.infn.it

we encounter the presumably fundamental Higgs field, whereas a composite mesonic scalar field serves as a useful effective degree of freedom for the description of the chiral QCD transition. We show that these scalar fields can be dealt with on the same footing yielding only a single effective field for the description of both chiral transitions.

As an advantage, we can study the region near the rapid crossover as a function of the microscopic parameters, allowing to quantify the strength of the crossover in terms of a pseudo-critical exponent. We argue that this exponent is a measure for the amount of fine-tuning needed on the microscopic level, thereby quantifying the naturalness problem. In our approach, we can thus also compute how much the naturalness problem in the electroweak sector is “alleviated” by the presence of the QCD sector.

Finally, our approach can be used to estimate the properties of a non-fine-tuned version of the standard model. For the case that chiral-symmetry breaking of QCD would dominate fermion mass generation and condensate formation, QCD would also generate masses for the electroweak gauge bosons [14–16] the value of which we estimate in the present work.

A special class of such models are those that would solve the hierarchy problem by requiring an enhanced symmetry, scale invariance, which is then dynamically broken by means of QCD-like dimensional transmutation. Typically, the mass spectrum generated by this Coleman-Weinberg mechanism is sensitive to the details of the bare Lagrangian at the UV scale  $\Lambda$ , that is to say to the marginal couplings such as the quartic Higgs coupling. Extracting an unambiguous prediction for the mass spectrum in these scale invariant Coleman-Weinberg scenarios then requires a UV completion being able to remove the UV cutoff and to reduce the freedom in the choice of these bare couplings. Still, the details of the translation between the marginal couplings and the IR mass spectrum and interactions remain nonperturbative. Thus, the study presented in this article can be conceived as a first step in this direction.

Rather than focusing straight ahead on the critical region of approximate scale invariance, whose precise definition at sizable gauge coupling is already a non-trivial problem, we address a more general survey of the phase diagram, aiming to provide an overall picture of how the two extremal scenarios, the pure-Yukawa sharp second-order phase transition and the pure QCD universal chiral symmetry breaking, can be reconciled and connected with an intermediate and less understood regime, featuring the interplay of several sources of symmetry breaking.

Our work uses methods of functional renormalization in order to deal with the nonperturbative aspects of the problem. Moreover, these methods give access to treat fields as effective degrees of freedom in a scale-dependent manner which is crucial to focus on the relevant fields and remove redundant field variables.

In the following, we introduce the various relevant

sectors of the standard model in Sect. II in order to motivate the model subset which we include in our quantitative analysis. Section III briefly summarizes the central renormalization group flow equations including the scale-dependent field transformations that facilitate a study of the interplay of the chiral transitions. The nature of the transitions is quantitatively studied in Sect. IV, containing most of our results. We conclude in Sect. V. Technical details and additional quantitative analyses are contained in the appendices.

## II. CHIRAL SYMMETRY BREAKING SECTORS OF THE STANDARD MODEL

We are mainly interested in the interplay between the two sectors of the standard model which are responsible for the fermion mass formation through chiral symmetry breaking. For the electroweak sector, the driving mechanism is controlled by the RG-relevant mass parameter of the Higgs potential, whereas the QCD sector is controlled by the marginally relevant non-Abelian gauge coupling. Also, we neglect the long-range effects of the electroweak gauge bosons associated to the  $U(1)_Y \times SU(2)_L$  symmetry. The latter are subleading with respect to gluons, even though the limit of vanishing weak and hypercharge gauge couplings is presumably not smooth; in the full system, the construction of observables therefore requires a more careful discussion [17–21]. By dropping the electroweak gauge sector, our study differs from those of other deformations of the standard model where the coupling strengths of the weak and strong sectors are shifted relative to each other [14, 22, 23]. We also ignore most of the flavor asymmetry of the quarks and leptons, accounting specifically for the third generation of quarks which are most strongly coupled to the Higgs field, and for the split between the top and bottom quarks.

Finally, we deal with the strong-coupling IR regime with the help of a somewhat minimalistic description that nevertheless gives us a qualitative and semi-quantitative access to the chiral transition. For this, we start from microscopic QCD and study the renormalization flow towards the quark-meson model [24, 25] along the lines familiar from functional RG studies [26–29]. In fact, the quark-meson model can quantitatively be matched to chiral perturbation theory [30, 31] as the low-energy limit of QCD. As argued below, the QCD-induced mesonic scalar field can in fact account also for the standard-model Higgs field by means of an appropriate identification of degrees of freedom and couplings.

### A. From QCD to the quark-meson model

The QCD sector of the standard model consists of a non-Abelian  $SU(N_c)$  gauge theory minimally coupled to  $N_f$  massless Dirac fermions (quarks) defined by the

(Euclidean) action

$$S = \int_x \bar{\psi}_i^a i \not{D}_{ij} \psi_j^a + \frac{1}{4} F_{\mu\nu}^z F^{\mu\nu}. \quad (1)$$

The fermions are described by  $\psi_i^a$ , where  $a, b = 1, \dots, N_f$  denote the flavor indices and  $i, j = 1, \dots, N_c$  the fundamental color indices. The covariant derivative  $D_{ij}^\mu$  in the fundamental representation of the group  $SU(N_c)$  couples quarks to the non-Abelian gauge bosons  $(A^\mu)_{ij}$  and is given by

$$D_{ij}^\mu = \partial^\mu \delta_{ij} - ig(A^\mu)_{ij}. \quad (2)$$

In general, we work with the physical values of  $N_c = 3$  colors and  $N_f = 6$  flavors. However, when focusing on the top-bottom family, we use  $N_f = 2$  as is appropriate for a single generation.

For the approach to the low-energy phase of QCD, we map the microscopic QCD sector defined by Eq. (1) onto the quark-meson model which we consider as a useful effective field theory for our purposes. We emphasize that we do not introduce any new independent parameter but extract the IR values of the quark-meson model parameters from the RG flow. The translation from the high- to the low-energy description proceeds most conveniently by studying the four-fermion interactions which are induced during the RG flow through quark and gluon fluctuations. For the sake of simplicity, we focus solely on the scalar-pseudoscalar channel in a point-like approximation. This is familiar from the Nambu-Jona-Lasinio model which can become critical at strong coupling and mediates chiral symmetry breaking [32]. At intermediate scales, we therefore work with the effective action

$$\Gamma = \int_x \left\{ \bar{\psi}_i^a i \not{D}_{ij} \psi_j^a + \frac{1}{4} F_{\mu\nu}^z F^{\mu\nu} + \frac{1}{2} \bar{\lambda}_\sigma \left[ (\bar{\psi}_i^a \psi_i^b)^2 - (\bar{\psi}_i^a \gamma_5 \psi_i^b)^2 \right] \right\}, \quad (3)$$

amended by a suitable gauge-fixing and ghost sector. Again, the four-fermion interaction  $\bar{\lambda}_\sigma$  is not used as a model parameter, but computed from the RG flow of the microscopic action.

Starting from the asymptotically free high energy domain, the gauge coupling grows towards the low energy regime [33, 34], subsequently also driving the four-fermion coupling  $\bar{\lambda}_\sigma$  to large values. This is indicative for the approach to chiral symmetry breaking and condensate formation. The corresponding composite scalar degrees of freedom appearing in the effective low-energy theory can be traced by means of a Hubbard-Stratonovich transformation. Introducing the auxiliary complex scalar field,

$$\varphi^{ab} = -i \frac{\bar{h}}{m^2} \bar{\psi}_i^b P_L \psi_i^a, \quad \varphi^{*ab} = -i \frac{\bar{h}}{m^2} \bar{\psi}_i^a P_R \psi_i^b, \quad (4)$$

we can translate the four-fermion interaction into a Yukawa interaction of the fermions with the new scalar

degrees of freedom. The resulting effective action includes the quark-meson effective theory,

$$\Gamma = \int_x \partial_\mu \varphi^{ab} \partial^\mu \varphi^{*ab} + U(\varphi, \varphi^\dagger) + \bar{\psi}_i^a i \not{D}_{ij} \psi_j^a + \frac{1}{4} F_{\mu\nu}^z F^{\mu\nu} + i \bar{h} \bar{\psi}_i^a [P_R \varphi^{ab} + P_L \varphi^{*ba}] \psi_i^b. \quad (5)$$

Again, the Yukawa coupling  $\bar{h}$  as well as the mesonic effective potential  $U$  do not contain free parameters, but are determined by the RG flow of QCD and thus governed by the gauge coupling. Clearly, this action still contains massless gluons, and will do so even after an IR massive decoupling of the quarks and mesons. Since we are interested in the chiral transition, the presence of free massless gluons in the deep IR of the model is not relevant. Of course, confinement and the Yang-Mills mass gap removes gluons from the physical IR spectrum.

This model is invariant under  $SU(N_f)_L \times SU(N_f)_R$  transformations, where these transformations act independently on the left- and right-handed spinor

$$\begin{aligned} \psi_R &\rightarrow U_R \psi_R, \\ \psi_L &\rightarrow U_L \psi_L, \end{aligned} \quad (6)$$

as well as on their conjugate transposed as

$$\begin{aligned} \bar{\psi}_R &\rightarrow \bar{\psi}_R U_R^\dagger, \\ \bar{\psi}_L &\rightarrow \bar{\psi}_L U_L^\dagger. \end{aligned} \quad (7)$$

The scalar field transforms as

$$\begin{aligned} \varphi &\rightarrow U_R \varphi U_L^\dagger, \\ \varphi^\dagger &\rightarrow U_L \varphi^\dagger U_R^\dagger. \end{aligned} \quad (8)$$

Additionally the model is invariant under a  $U(1)_B$  symmetry, corresponding to baryon number conservation. It acts only on the spinor, since the scalar fields are made up of quark-antiquark pairs (c.f. Eq. (4)) and thus carry no baryon number

$$\begin{aligned} \psi &\rightarrow \exp\left(\frac{i\vartheta_B}{3}\right) \psi \\ \bar{\psi} &\rightarrow \exp\left(-\frac{i\vartheta_B}{3}\right) \bar{\psi}. \end{aligned} \quad (9)$$

The  $U(1)_A$  anomaly could be included in the present framework [26, 35–39], but is not relevant for our purposes. Chiral symmetry breaking in this model induces a non-vanishing vacuum expectation value for the scalar field. The phenomenologically relevant breaking pattern corresponds to the vacuum configuration

$$\varphi_0 = \begin{pmatrix} \sigma_0 & 0 & \dots & 0 \\ 0 & \sigma_0 & \dots & 0 \\ \vdots & \vdots & \ddots & \vdots \\ 0 & 0 & \dots & \sigma_0 \end{pmatrix}, \quad (10)$$

which breaks the  $SU(N_f)_L \times SU(N_f)_R$  symmetry of the model down to the diagonal  $SU(N_f)_V$  subgroup.

In this case we consider a quartic approximation for the scalar potential, in the symmetric (SYM) and in the spontaneous-symmetry-breaking (SSB) regimes, respectively given by

$$\begin{aligned} U(\varphi, \varphi^\dagger) &= m^2 \varrho + \frac{1}{2} \lambda_1 \varrho^2 + \frac{1}{4} \tau, & \text{SYM,} \\ U(\varphi, \varphi^\dagger) &= \frac{1}{2} \lambda_1 (\varrho - \varrho_0)^2 + \frac{1}{4} \tau, & \text{SSB,} \end{aligned} \quad (11)$$

where we have introduced the invariants

$$\begin{aligned} \varrho &= \text{tr}(\varphi^\dagger \varphi), \\ \tau &= 2 \text{tr}(\varphi^\dagger \varphi)^2 - \varrho^2. \end{aligned} \quad (12)$$

Here  $\varrho_0$  denotes the scale-dependent minimum of the scalar potential in the SSB regime. The scalar mass spectrum obtained by spontaneous chiral symmetry breaking with the vacuum configuration given by Eq. (10) is given in appendix B, and has been discussed in detail for general  $N_f$  in ref. [40, 41]

### B. Identifying the overlap of the Higgs and meson degrees of freedom

The auxiliary meson field  $\varphi$  introduced in the low-energy effective description of strong interactions, and the fundamental Higgs doublet  $\phi$  of the standard model play similar roles, as their vacuum expectation value parametrizes mass generation and chiral symmetry breaking. This similarity poses fundamental questions, which are ultimately connected with the challenge of bridging between effective field theories valid at very different scales. See for instance refs. [42, 43] for discussions of the possible interplay of these two fields.

The quark meson model is generically conceived as an effective description of the strong interactions below energies of the order of a few GeV, with a characteristic scale of breaking of the approximate chiral symmetry given by the vacuum expectation value  $v$  of the  $\sigma$  field, Eq. (10), of the order of  $f_\pi \simeq 93$  MeV. An effective UV cutoff scale – if it exists – of the Higgs model is instead unknown. In the present work, we parametrize it by a high-energy scale  $\Lambda$  which we take as sufficiently large. Towards lower scales, the parameters of the Higgs potential generate the electroweak scale, characterized by the breaking of the global  $SU(2)_L \times SU(2)_R$  custodial symmetry and of the exact chiral symmetry at the characteristic Fermi scale of  $\Lambda_F = 246$  GeV. The Fermi scale at the same time corresponds to the vacuum expectation value  $v$  of the Higgs field. From this point of view there seems to be no reason to aim at the simultaneous description of the two phenomena by means of a single linear sigma model.

Following this perspective, a first investigation of the electroweak phase transition in a chiral Higgs-top-bottom model has been studied in Ref. [44] and is summarized in appendix C. This study adopts RG methods, along the lines for instance of Ref. [8], and supplements

the quark-meson model with an independent elementary Higgs field.

As a matter of fact however, the effective descriptions of symmetry breaking by the two sigma models describing the strong and the Higgs sectors are indistinguishable, as the relevant corresponding components of the scalar fields carry the same conserved quantum numbers (also in presence of the full electroweak gauge sectors). Therefore, we focus here on the simplest toy model, where we remove the redundant double-counting of the parity-even scalar symmetry-breaking channel. In the present Higgs-QCD model it is particularly clear that the overlap between the QCD meson field and the Higgs sectors extends even beyond the single degrees of freedom describing the sigma and Higgs particles, and can include the whole Higgs doublet. Of course with doublet here we mean a fundamental representation of the global  $SU(2)_L$  group only, which is a subgroup of the QCD chiral symmetry, as the electroweak gauge sector of the standard model is not taken into consideration in the present analysis.

In order to make this matching of the scalar degrees of freedom explicit, we focus in the following on the 3rd generation of quarks, the top and bottom family for which we reduce our equations to  $N_f = 2$ . The identification of the Higgs doublet with some of the components of the collective QCD-meson field becomes transparent from an analysis of the Yukawa interactions. Using a reparametrization of the meson field as

$$\begin{aligned} \Phi^{ab} &= \frac{1}{\sqrt{2}} \left( \varphi^{ab} + \epsilon^{ac} \epsilon^{bd} \varphi^{*cd} \right) \\ \tilde{\Phi}^{ab} &= \frac{1}{\sqrt{2}} \left( \varphi^{*ab} - \epsilon^{ac} \epsilon^{bd} \varphi^{cd} \right), \end{aligned} \quad (13)$$

we find that each scalar field  $\Phi$  and  $\tilde{\Phi}$  contains 4 real degrees of freedom for the present case of  $N_f = 2$ , and the various components can be related under complex conjugation through

$$\begin{aligned} \Phi^{*ab} &= \epsilon^{ac} \epsilon^{bd} \Phi^{cd} \\ \tilde{\Phi}^{*ab} &= -\epsilon^{ac} \epsilon^{bd} \tilde{\Phi}^{cd}. \end{aligned} \quad (14)$$

These fields transform under the  $(\mathbf{2}, \mathbf{2})$  representation of the  $SU(2)_L \times SU(2)_R$  symmetry group.

$$\begin{aligned} \Phi &\rightarrow U_L \Phi U_R^\dagger \\ \tilde{\Phi} &\rightarrow U_R^\dagger \tilde{\Phi} U_L. \end{aligned} \quad (15)$$

The conventional electroweak Higgs field  $\phi^a$  as a complex doublet can be identified by

$$\phi^a \equiv \Phi^{a2}, \text{ implying } \phi_C^a = i(\sigma_2)^{ab} \phi^{*b}. \quad (16)$$

As required,  $\phi^a$  transforms under  $SU(2)_L$ . In addition, we can define  $\tilde{\phi}^a$  as a complex doublet under  $SU(2)_R$  by

$$\tilde{\phi}^a = \tilde{\Phi}^{2a}, \text{ implying } \tilde{\phi}_C^a = -i(\sigma_2)^{ab} \tilde{\phi}^{*b}, \quad (17)$$

respectively. This allows us to rewrite the Yukawa interaction in the quark-meson model as

$$\mathcal{L}_{\text{Yuk}}^{\text{QM}} = \frac{i\bar{h}}{\sqrt{2}} \left( \bar{\psi}_{L,i}^a \phi^a b_{R,i} + \bar{\psi}_{L,i}^a \phi_C^a t_{R,i} + \text{h.c.} \right. \\ \left. + \bar{\psi}_{R,i}^a \tilde{\phi}^a b_{L,i} + \bar{\psi}_{R,i}^a \tilde{\phi}_C^a t_{L,i} + \text{h.c.} \right). \quad (18)$$

Here we have used the following standard notation for the flavor components of the fermion field

$$\psi_{L/R,i} = \begin{pmatrix} t_{L/R,i} \\ b_{L/R,i} \end{pmatrix}. \quad (19)$$

Comparing this Yukawa interaction with the one of the Higgs-top-bottom model for the special case  $N_f = 2$ , we observe the scalar field  $\phi$  to have the same quantum numbers as the Higgs doublet, while the  $\tilde{\phi}$  field contains the remaining four real degrees of freedom present in the mesonic field of QCD (for  $N_f = 2$ ). The latter has no analogue in the electroweak sector, and here describes a doublet in the fundamental representation of  $SU(2)_R$ .

As quarks in the standard model have nonvanishing electroweak charges, four-Fermi couplings exist in several channels with a complicated charge assignment. The channels which are related to the Higgs field upon a Hubbard-Stratonovich transformation are well known from top quark condensation models [45–48]. Independently of the details, the corresponding channels always have some overlap with the QCD induced channels. After a Hubbard-Stratonovich transformation, we match those parts of the mesonic field that share the same quantum numbers with the Higgs field.

Although meson Yukawa couplings emerge as an effective description of the quark four-fermion couplings induced by QCD, the standard model features also fundamental Yukawa couplings to the Higgs. As a consequence, we introduce new coupling constants for the top and bottom Yukawa interaction and arrive at the final form

$$\mathcal{L}_{\text{Yuk}} = \frac{i\tilde{h}_b}{\sqrt{2}} \left( \bar{\psi}_{L,i}^a \phi^a b_{R,i} + \bar{b}_{R,i} \phi^{*a} \psi_{L,i}^a \right) \\ + \frac{i\tilde{h}_t}{\sqrt{2}} \left( \bar{\psi}_{L,i}^a \phi_C^a t_{R,i} + \bar{t}_{R,i} \phi_C^{*a} \psi_{L,i}^a \right) \\ + \frac{i\bar{h}}{\sqrt{2}} \left( \bar{\psi}_{R,i}^a \tilde{\phi}^a b_{L,i} + \bar{\psi}_{R,i}^a \tilde{\phi}_C^a t_{L,i} + \text{h.c.} \right), \quad (20)$$

where

$$\tilde{h}_{t/b} = \bar{h}_{t/b} + \bar{h}. \quad (21)$$

Despite the simple new parametrization of Eq. (21), it is important to stress that the flow of the couplings  $\tilde{h}_{t/b}$  is primarily driven by the electroweak sector, whereas  $\bar{h}$  is driven by QCD fluctuations. Notice also that the interaction of the  $SU(2)_R$ -doublet  $\tilde{\phi}$  with the quarks remains fully parametrized by the QCD-induced coupling  $\bar{h}$ .

The model inherits the  $U(1)_B$  symmetry of Eq. (9) from the quark meson model, corresponding to baryon number conservation in the theory. (NB: we ignore the  $U(1)_B$  violating sphaleron processes of the standard model in our analysis.)

While we have focused here on the top/bottom family, the matching of the scalar fields also applies to the lighter quark families as the corresponding sectors in the mesonic field carries the same quantum numbers. In this manner, the current quark masses are generated at the Fermi scale from the corresponding fundamental Yukawa couplings. The main difference, however, is that the lighter quarks do not decouple near the Fermi scale and thus the corresponding mesonic fields are predominantly driven more and more by QCD. In addition, the full mesonic field also contains components that link the different families to one another. These inter-family components do not correspond to any part of the electroweak Higgs field.

### C. From the meson potential to the Higgs phase

We now want to construct a scalar potential out of the invariants of the fields  $\phi$  and  $\tilde{\phi}$ ,

$$\rho = \phi^\dagger \phi, \\ \tilde{\rho} = \tilde{\phi}^\dagger \tilde{\phi}. \quad (22)$$

The  $SU(2)_L \times SU(2)_R$  invariant  $\varrho$  defined in Eq. (12) then yields

$$\varrho = \rho + \tilde{\rho}. \quad (23)$$

A particular quartic potential constructed out of these invariants and inspired by Eq. (11) is given by

$$U(\rho, \tilde{\rho}) = m^2 (\rho + \tilde{\rho}) + \frac{\lambda_1}{2} (\rho + \tilde{\rho})^2 + \lambda_2 \rho \tilde{\rho}. \quad (24)$$

This potential, however, cannot be mapped one-to-one to the scalar potential given in (11), since the  $\tau$  invariant cannot be expressed by  $\rho$  and  $\tilde{\rho}$  alone. This mismatch between Eq. (24) and Eq. (11) has a subdominant effect on the scalar spectrum, which slightly differs in the two cases as is discussed in appendix B.

In the symmetric case where  $m^2 > 0$ , the minimum of the potential has a vanishing field,  $\rho = 0$  and  $\tilde{\rho} = 0$ . In the symmetry-breaking regime, we parametrize the potential by

$$U(\rho, \tilde{\rho}) = \frac{\lambda_1}{2} (\rho + \tilde{\rho} - \kappa)^2 + \lambda_2 \rho \tilde{\rho}. \quad (25)$$

For being able to describe the standard-model-like Higgs phase, we specify our vacuum to be  $\rho = \kappa$  and  $\tilde{\rho} = 0$ . The vacuum expectation value in the  $\phi$  field spontaneously breaks the  $SU(2)_L \times SU(2)_R$  symmetry of the QCD part of the model down to diagonal  $SU(2)$  and induces Dirac masses for the fermions through the Yukawa

interaction. Choosing our vacuum to be

$$\phi|_{\text{vac}} = \begin{pmatrix} 0 \\ \sqrt{\kappa} \end{pmatrix}, \quad \tilde{\phi}|_{\text{vac}} = \begin{pmatrix} 0 \\ 0 \end{pmatrix}, \quad (26)$$

the induced fermion masses read

$$m_{\text{top}}^2 = \frac{\tilde{h}_t^2}{2}\kappa, \quad m_{\text{bot}}^2 = \frac{\tilde{h}_b^2}{2}\kappa. \quad (27)$$

The scalar spectrum contains  $N_f^2 - 1$  massless degrees of freedom (Goldstone bosons),  $N_f^2$  degrees of freedom with mass  $\sqrt{\lambda_2\kappa}$  and one radial mode corresponding to the Higgs particle with mass  $\sqrt{2\lambda_1\kappa}$ . For conventional applications in the quark-meson model with  $N_f = 2$  light (first generation) quark flavors, the three Goldstone modes are identified with the pions. In the present setting, where we consider the third generation, the  $\phi$  field corresponds to the Higgs instead. Upon embedding into the full standard model, the gauged  $SU(2)_L$  provides mass to the corresponding gauge bosons through the Brout-Englert-Higgs mechanism and the Goldstone bosons disappear. In the present simplified model, these massless Goldstone bosons would naively remain in the spectrum. In order to avoid artifacts caused by them, we decouple them from the flow by giving them a mass of the order of the longitudinal gauge bosons, once the Higgs field develops a vacuum expectation value near the Fermi scale.

### III. RG FLOW EQUATIONS

Effective field theories are a perfect tool for the description of phase transitions, as is well established since the early work of Ginzburg and Landau. However, to address issues such as decoupling of degrees of freedom, hierarchy of scales, or even the origin of symmetry breaking, they have to be complemented with additional information. RG methods are often the preferred source of this information. To be able to follow the RG flow of our effective toy model from its weak-coupling standard-model-like UV behavior down to the chiral-symmetry-breaking regime, we need nonperturbative methods. The precise running of the strong gauge coupling and the details of the QCD IR dynamics are not essential for our main case study of the interplay of the chiral transitions. We therefore model the gauge flow with a simple ansatz for the running gauge coupling described in the following. On the other hand, the influence that this strongly coupled gauge sector has on the matter fields and especially on the Higgs-meson sector is of crucial relevance. For the latter, we resort to functional RG methods whose description and implementation is the main body of this section.

#### A. Gauge sector

In the gauge sector, we use a perturbative two-loop equation for the running of the gauge coupling. We im-

prove this flow such that we obtain an IR fixed point  $\alpha_* = g_*^2/(4\pi)$  for that coupling, whose presence e.g. in Landau gauge has been put forward by a number of studies, see for instance refs. [49–55]. In the FRG scheme that we are using, such a fixed point is rather generic as it is compatible with the decoupling of IR modes due to confinement and mass gap generation. This fixed point has to be chosen above the critical gauge coupling needed to induce chiral symmetry breaking [56–60]. The precise choice of  $\alpha_*$  is then irrelevant for our analysis, since massive hadronic freeze-out occurs before the fixed-point regime. Although capturing chiral symmetry breaking, this *ad hoc* modification of the beta function together with the restriction to point-like fermionic self-interactions is a somewhat crude approximation which can be substantially improved within a systematic propagator and vertex expansion [61–65].

We describe the scheme-dependent intermediate flow between the perturbative weakly coupled regime and the nonperturbative fixed point by means of a smooth exponential function [56]. Other parametrizations, for instance using a Heaviside step function as the opposite extreme, would not significantly change our results. The beta function for the gauge coupling then reads

$$\begin{aligned} \partial_t g^2 = \eta_F g^2 = & -2 \left( c_1 \frac{g^4}{16\pi^2} + c_2 \frac{g^6}{(16\pi^2)^2} \right) \\ & \times \left( 1 - \exp\left( \frac{1}{\alpha_*} - \frac{1}{\frac{g^2}{4\pi}} \right) \right), \end{aligned} \quad (28)$$

where we have introduced the constants

$$\begin{aligned} c_1 &= \left( \frac{11}{3} N_c - \frac{2}{3} N_f \right), \\ c_2 &= \left( \frac{34}{3} N_c^2 - \frac{10}{3} N_c N_f - 2C_2(N_c) N_f \right). \end{aligned} \quad (29)$$

At high energies, we use  $N_f = 6$  active flavors within the beta function but dynamically account for their decoupling across their mass thresholds for the heavy quarks. After crossing into the broken regime at  $k = k_{\text{trans}}$ , we gradually switch off the top and bottom quark in the running of the strong gauge coupling by decreasing the effective number of active flavors to 5 at the top mass threshold, and then to 4 at the bottom threshold. The thresholds of both quarks are determined by their respective Yukawa coupling at the transition scale

$$m_t^2 \approx \frac{1}{2} \tilde{h}_t^2|_{k=k_{\text{trans}}} k_{\text{trans}}^2, \quad m_b^2 \approx \frac{1}{2} \tilde{h}_b^2|_{k=k_{\text{trans}}} k_{\text{trans}}^2. \quad (30)$$

Expressed through RG time, we decouple the quarks from the running of the strong gauge coupling at

$$t_{\text{top}} = \ln\left( \frac{\tilde{h}_t}{\sqrt{2}} \right) \quad \text{and} \quad t_{\text{bottom}} = \ln\left( \frac{\tilde{h}_b}{\sqrt{2}} \right) \quad (31)$$

after we entered the broken regime.

## B. Matter sector

We study the matter sector of our model using the functional renormalization group (FRG) as a method that allows us to address strong-coupling regimes as well as the perturbative accessible weak-coupling limit. The starting point is a (bare) microscopic action  $S$  defined at an UV cutoff  $\Lambda$  and the RG flow of a scale-dependent effective action  $\Gamma_k$  given by the Wetterich equation [66–69]

$$\partial_t \Gamma_k = \frac{1}{2} \text{STr} \left( \frac{\partial_t R_k}{\Gamma_k^{(2)} + R_k} \right). \quad (32)$$

This scale-dependent effective action interpolates between the bare action  $\Gamma_{k=\Lambda} = S$ , and the full quantum effective action  $\Gamma_{k=0} = \Gamma$ , where all quantum corrections have been integrated out. In Eq. (32)  $R_k$  denotes the regulator, which is to some extent an arbitrary function of momentum. Its additive insertion in the denominator (i.e. in the exact propagator) serves as an IR cutoff for momenta smaller than  $k$ . On the other hand, the derivative  $\partial_t R_k$  in the numerator is chosen to provide UV regularisation of the trace integral. Despite its simple closed one-loop form, Eq. (32) can be proved to be exactly equivalent to the standard functional-integral definition of  $\Gamma$  in presence of a mass-like deformation  $R_k$  in the bare action. This exactness, combined with systematic approximation schemes like the derivative expansion or the vertex expansion, turns Eq. (32) into a useful nonperturbative tool, which has been extensively applied to a wide selection of problems in quantum, statistical, or many body physics. For more details we direct the interested reader to the rich secondary literature [70–75].

For the application of the FRG equation, we project the exact equation (32) onto the ansatz derived in the previous section, specifically Eq. (5) with the field redefinition that leads to the standard-model-like Yukawa interactions of Eq. (20). This can be understood as a leading order of the derivative expansion for the quantum effective action. Additionally we allow for a scale-dependent kinetic term of the fields by introducing a wave-function-renormalization factor for each field. The gauge coupling, the scalar potential  $U$ , the Yukawa couplings, and the wave function renormalizations for the various fields  $Z_i$  are all scale dependent; we suppress the index  $k$  often used to denote scale-dependent quantities for notational clarity. Using this truncation in the Wetterich equation and projecting onto the respective operators yields the  $\beta$  functions for their couplings.

We account for the running of the wave-function renormalizations through the so-called anomalous dimensions of the respective fields,

$$\eta_i = -\partial_t \log Z_i. \quad (33)$$

Furthermore it is useful to introduce dimensionless,

renormalized quantities as

$$\begin{aligned} \rho &= Z_\phi k^{2-d} \phi^\dagger \phi, & \tilde{\rho} &= Z_{\tilde{\phi}} k^{2-d} \tilde{\phi}^\dagger \tilde{\phi}, \\ h_t &= Z_\phi^{-1} Z_L^{-1} Z_R^t^{-1} \tilde{h}_t, & h_b &= Z_\phi^{-1} Z_L^b^{-1} Z_R^b^{-1} \tilde{h}_b, \\ h^2 &= Z_{\tilde{\phi}}^{-1} Z_L^{t-1/2} Z_L^{b-1/2} Z_R^{t-1/2} Z_R^{b-1/2} \tilde{h}^2. \end{aligned} \quad (34)$$

For concrete computations, we work in  $d = 4$  later on. We also employ the Landau gauge, where the gauge parameter is set to zero. This gauge choice is known to be a fixed point of the RG flow of the gauge-fixing parameter [76–78]. Using standard calculation techniques [70], we extract the flow equations and obtain for the scalar potential

$$\begin{aligned} \partial_t u &= -du + (d-2 + \eta_\phi) \rho u_\rho + (d-2 + \eta_{\tilde{\phi}}) \tilde{\rho} u_{\tilde{\rho}} \\ &+ v_d \left\{ 3l_0^d (\mu_G^2; \eta_\phi) + l_0^d (\mu_H^2; \eta_\phi) \right. \\ &\quad \left. + 3l_0^d (\mu_m^2; \eta_{\tilde{\phi}}) + l_0^d (\mu_{m,r}^2; \eta_{\tilde{\phi}}) \right\} \\ &- 2d_\gamma N_c v_d \left\{ l_0^{(F)d} (\mu_t^2; \eta_t) + l_0^{(F)d} (\mu_b^2; \eta_b) \right\}, \end{aligned} \quad (35)$$

where subscripts in  $u$  denote derivatives with respect to the corresponding variable. The various threshold functions  $l_0^d, l_0^{(F)d}$  etc. responsible for the decoupling of massive modes can be found in the appendix D for the special choice of the linear regulator [79]. In Eq. (35),  $d_\gamma$  is the dimension of the spinor representations of the fermions, and  $v_d^{-1} = 2^{d+1} \pi^{d/2} \Gamma(d/2)$ . We have also introduced the abbreviations

$$\begin{aligned} \mu_t^2 &= \frac{h_t^2}{2} \rho + \frac{h^2}{2} \tilde{\rho}, \\ \mu_b^2 &= \frac{h_b^2}{2} \rho + \frac{h^2}{2} \tilde{\rho}, \\ \mu_G^2 &= u_\rho, \\ \mu_H^2 &= u_\rho + 2\rho u_{\rho,\rho}, \\ \mu_m^2 &= u_{\tilde{\rho}}, \\ \mu_{m,r}^2 &= u_{\tilde{\rho}} + 2\tilde{\rho} u_{\tilde{\rho},\tilde{\rho}}. \end{aligned} \quad (36)$$

We simplify the task of following the RG evolution of the full effective potential by means of a quartic polynomial truncation, adopting the parametrizations of Eq. (24) and Eq. (25) in the SYM and in the standard-model-like SSB regimes respectively. A more general functional analysis of the scalar potential would be able to fully describe all possible SSB regimes [80, 81]. The remaining flow equations of the model can be found in the App. A.

## C. Partial Bosonization

For our scale-dependent analysis, the Hubbard-Stratonovich transformation (4) which translates our four-fermion interaction into a Yukawa interaction between quarks and mesons needs to be treated dynamically: If we translated the full four-fermion interaction

into the scalar sector at a fixed matching scale  $k_m$ , gluonic fluctuations would generate a nonzero four-fermion coupling again at scales  $k < k_m$ . To fully account for these radiatively generated interactions, we apply the bosonization prescription continuously, i.e. at every scale  $k$ . To this end we promote the scalar field to be scale dependent, reabsorbing the four-fermion interaction into the scalar sector for all  $k$ . This yields additional contributions to the flow equation of the effective average action [72, 82–86]

$$D_t \Gamma_k[\varphi_k] = \partial_t \Gamma_k[\varphi_k] \Big|_{\varphi_k} - \int_x \frac{\delta \Gamma_k[\varphi_k]}{\delta \varphi_k} \partial_t \varphi_k, \quad (37)$$

The first term on the right-hand side accounts for the RG flow of the model of Eq. (3), without dynamical re-bosonization. The second term takes the new scale dependence of the fields into account and ensures a vanishing fermionic self-interaction on all scales. In order to keep the concrete computations simple, we use the approximative scheme of [56, 82]. See refs. [71, 73] for an introduction to this method.

We choose the following ansatz for the scale dependence of the scalar field

$$\begin{aligned} \partial_t \varphi_k^{ab}(q) &= -i (\bar{\psi}^b P_L \psi^a)(q) \partial_t \alpha_k(q) + \varphi^{ab} \partial_t \beta_k(q), \\ \partial_t \varphi^{*ab}(q) &= -i (\bar{\psi}^a P_R \psi^b)(-q) \partial_t \alpha_k(q) + \varphi^{*ab} \partial_t \beta_k(q), \end{aligned} \quad (38)$$

with  $\alpha_k(q)$  and  $\beta_k(q)$  being functions to be chosen such that our four fermion coupling stays zero for the full flow [56, 71, 82]. The scale dependence of the meson scalar fields, descending from Eq. (38), entails a corresponding scale dependence of the Higgs (left-charged) and dual-Higgs (right-charged) scalar doublets, which can be straightforwardly computed from the linear field transformation (14).

The scale dependence of the scalar field, together with the second term in Eq. (37), yields additional contributions to the flow equations, specifically to the flow of the Yukawa coupling  $h$  and the scalar potential  $u$ . Recall that our parametrization of the Yukawa couplings shown in Eq. (20) assumes a simple linear superposition of the meson-like and fundamental Higgs-like couplings, see Eq. (21). Correspondingly, we capture the effects of the scale-dependent partial bosonization solely in the meson-like Yukawa coupling  $h$ . This is of course a simple modeling of a more intricate structure of higher-dimensional operators mixing the quarks, the Higgs and the mesons.

In the symmetric regime, the additional contribution to the (dimensionless) mass parameter in the scalar potential is conveniently expressed in terms of the ratio

$$\epsilon = \frac{m^2}{k^2 h^2}, \quad (39)$$

and given by [56]

$$\partial_t \epsilon \Big|_{\text{d.b.}} = 2 \frac{\epsilon}{h^2} (1 + \epsilon) (1 + (1 + \epsilon) Q_\sigma) (\beta_{\lambda_\sigma}^{g^4} g^4 + \beta_{\lambda_\sigma}^{g^2 h^2} g^2 h^2), \quad (40)$$

where  $\# \Big|_{\text{d.b.}}$  denotes the additional contributions stemming from dynamical bosonization (the second term in (37)), while the Yukawa contribution reads

$$\partial_t h^2 \Big|_{\text{d.b.}} = 2(1 + 2\epsilon + Q_\sigma(1 + \epsilon)^2) (\beta_{\lambda_\sigma}^{g^4} g^4 + \beta_{\lambda_\sigma}^{g^2 h^2} g^2 h^2). \quad (41)$$

In the broken regime, we similarly find

$$\begin{aligned} \partial_t \kappa \Big|_{\text{d.b.}} &= 2 \frac{\kappa}{h^2} (1 - \kappa \lambda_1) (1 + (1 - \kappa \lambda_1) Q_\sigma) \\ &\quad \times (\beta_{\lambda_\sigma}^{g^4} g^4 + \beta_{\lambda_\sigma}^{g^2 h^2} g^2 h^2) \end{aligned} \quad (42)$$

as the additional contribution to the running of the (dimensionless) minimum of the potential, and

$$\partial_t h^2 \Big|_{\text{d.b.}} = 2(1 - 2\kappa \lambda_1 + Q_\sigma(1 - \kappa \lambda_1)^2) (\beta_{\lambda_\sigma}^{g^4} g^4 + \beta_{\lambda_\sigma}^{g^2 h^2} g^2 h^2) \quad (43)$$

for the Yukawa coupling in the SSB regime. Here we have used

$$\begin{aligned} \beta_{\lambda_\sigma}^{g^4} &= -\frac{1}{4} \frac{9N_c^2 - 24}{N_c} v_d l_{1,2}^{(\text{FB})d}(0, 0; \eta_\psi, \eta_F), \\ \beta_{\lambda_\sigma}^{g^2 h^2} &= \frac{48}{N_c} v_d l_{1,1,1}^{(\text{FBB})d}(0, \epsilon, 0; \eta_\psi, \eta_\phi, \eta_F), \end{aligned} \quad (44)$$

for brevity.

The quantity  $Q_\sigma = \partial_t (\bar{\lambda}_\sigma(k^2) - \bar{\lambda}_\sigma(0)) / \partial_t \bar{\lambda}_\sigma(0)$  measures the suppression of the four-fermion coupling  $\bar{\lambda}_\sigma$  for large external momenta and is, in principle, straightforwardly computable. A suppression implies  $Q_\sigma < 0$ . In the SSB regime, where fermions are massive, non-pointlike four-fermion interactions are suppressed by the inverse fermion mass squared coming from the two internal propagators [87]. Therefore we choose the ansatz

$$Q_\sigma = \frac{Q_\sigma^0}{2} \left( m_{1,2}^{(\text{FB})d}(\mu_t^2, 0; \eta^t, \eta_F) + m_{1,2}^{(\text{FB})d}(\mu_b^2, 0; \eta^b, \eta_F) \right) \quad (45)$$

which has the right decoupling properties but introduces a free parameter  $Q_\sigma^0$ . Tests for various different values of  $Q_\sigma^0 \in [-0.5, 0]$  show that results are qualitatively independent of the precise choice of this parameter [44, 56].

#### D. Evaluation of the RG flows

As a check of the reliability of our approximations, we compare the so-called local potential approximation (LPA), where all anomalous dimensions of the fields are neglected, to the generalization including the running wave function renormalizations of the fields (sometimes called LPA'). This check confirms the stability of our main results, that we present in the next section.

Furthermore and as mentioned above, our reduction of the standard model comes with some artifacts such as unphysical massless modes. As argued above, the massless gluons do not affect the chiral transitions and can therefore safely be ignored. By contrast, the massless would-be Goldstone bosons of the Higgs field in

the SSB regime would induce an unphysical logarithmic flow. We cure this artifact by introducing masses in the SSB regime for these modes in order to model the Brout-Englert-Higgs (BEH) mechanism in the full model following the prescription of [8]. As studied in more detail in Ref. [44] and substantiated for the present work in App. B, this procedure has little to no influence on the IR values of interest in this study.

Finally, we comment on a subtlety related to the different parametrizations of the scalar potential elucidated in Sect. II. The parametrization Eq. (24) of the potential differs from that of Eq. (11), as the invariant  $\tau$  cannot be expressed in terms of  $\rho$  and  $\tilde{\rho}$ . This leads to a slightly different scalar mass spectrum in the two cases. Because of the different spectrum, the RG flow equation for the coupling  $\lambda_2$  in the potential differs from the one found in the quark meson model (see for instance refs. [40, 70]). For simplicity, we adopt the beta function of  $\lambda_2$  stemming from the quark-meson model and the potential parametrization (11), with the correct thresholds corresponding to the scalar mass spectrum arising from Eq. (24). The consistency of this approach is confirmed by the stability of the results shown below. In fact, implementing the RG equation coming directly from the form of Eq. (24) would just change the IR value of the  $\lambda_2$  coupling by a small amount, affecting only the masses of the  $SU(2)_R$  doublet. By contrast, the effects we are interested in do not depend on  $\lambda_2$ .

#### IV. NATURE OF THE CHIRAL TRANSITION

Let us now investigate the nature of the chiral transitions within our parametrization of the essential standard model sectors. More specifically, we are interested in studying the transitions as a function of the microscopic (bare) parameters. From an RG perspective, the most RG-relevant parameter that gives access to both sides of the transition can serve as a control parameter to explore the near critical regime.

Let us start from the limiting case, where we consider only the Higgs-top-bottom Yukawa sector. This sector exhibits a behavior reminiscent to a second-order chiral quantum phase transition with the mass parameter of the Higgs potential serving as a control parameter [8]. In the language of critical phenomena [88], the chiral order parameter corresponding to the Higgs expectation value scales in the ordered (broken) phase near criticality according to a power law

$$\langle \phi \rangle \propto |t|^\beta, \quad (46)$$

where  $\beta$  denotes a critical exponent, and  $t$  corresponds to the reduced temperature in a thermodynamic setting, (for quantum phase transitions, the corresponding control parameter is often called  $\delta$ ). In the present model, the control parameter can be identified as

$$t = \epsilon - \epsilon_* \equiv \delta\epsilon_\Lambda, \quad (47)$$

where  $\epsilon_*$  denotes the critical value of the dimensionless mass parameter of the Higgs potential at the UV cutoff  $\Lambda$  separating the different phases. The precise value depends on all other bare couplings as well as on the RG scheme, but the deviation  $\delta\epsilon_\Lambda$  is a suitable choice as an analogue for the reduced temperature.

By means of so-called scaling and hyperscaling relations [88], the critical exponent  $\beta$  can be related to two other thermodynamic exponents used to describe the power law behaviour of the correlation length, as well as the anomalous dimension exponent  $\eta$

$$\beta = \frac{\nu}{2} (d - 2 + \eta). \quad (48)$$

Here  $\eta$  corresponds to the anomalous dimension coming from the wave function renormalization evaluated at the critical point. Thus, it describes the long-range behavior of the correlation function ( $\langle \phi(0)\phi(r) \rangle \propto r^{-d+2-\eta}$ ) when the correlation length diverges. In addition, we encounter the correlation length exponent  $\nu$ . Using the RG approach to the theory of critical phenomena, we can relate this critical exponent  $\nu$  to the RG scaling exponent  $\Theta$  of the most relevant perturbation at the critical point by

$$\nu = \frac{1}{\Theta}. \quad (49)$$

At small interactions, i.e., near the Gaussian fixed point, the mass parameter of the Higgs potential is the most relevant perturbation, with its dimensionless version  $\epsilon$  scaling as  $\epsilon \sim k^{-2} =: k^{-\Theta}$ , cf. Eq. (39), such that  $\Theta = 2$  characterizes the non-interacting limit. Hence,  $\Theta$  denotes the power-counting dimension of the scalar mass parameter, and reflects its quadratic running tied to the naturalness problem: in presence of a high energy scale such as a UV cutoff  $\Lambda$  and assuming all bare parameters to be of order 1 at this scale, physical dimensionful long-range observables, like the vacuum expectation value of the scalar field (the Fermi scale), are expected to be of the same order of magnitude of  $\Lambda$ . Much smaller values are possible only at the expense of an exceptional amount of fine-tuning of the bare parameters at the scale  $\Lambda$  such that bare parameters and contributions from quantum fluctuations cancel to a high degree.

In the vicinity of the Gaussian fixed point, perturbation theory predicts corrections to the canonical scaling yielding

$$\Theta = 2 - \eta, \quad (50)$$

which – upon expansion – leads to at most logarithmic corrections to canonical scaling in accordance with Weinberg's theorem. Upon insertion of Eq. (50) into Eq. (48), we find

$$\beta = \frac{1}{2} \left( 1 + \eta + \frac{1}{2}\eta^2 + \mathcal{O}(\eta^3) \right). \quad (51)$$

for the scaling of the order parameter.

Let us illustrate this using the quantum phase transition of the reduced Higgs-top-bottom model. For otherwise fixed couplings, the vacuum expectation value of the Higgs field in this ungauged model is shown in Fig. 1 as a function of the control parameter  $\delta\epsilon_\Lambda$ . For positive values of the control parameter, the model is in the symmetric phase  $v = 0$ . For negative values, the order parameter  $v$  increases rapidly according to the scaling law (46). Since the model is comparatively weakly coupled, we expect the critical exponents to be close to their *mean-field* values  $\beta \simeq 1/2$  and  $\eta \simeq 0$ . (More precisely, the top-Yukawa coupling as the largest coupling introduces sizable quantum corrections such that  $\eta \simeq 0.07$ , see below.)

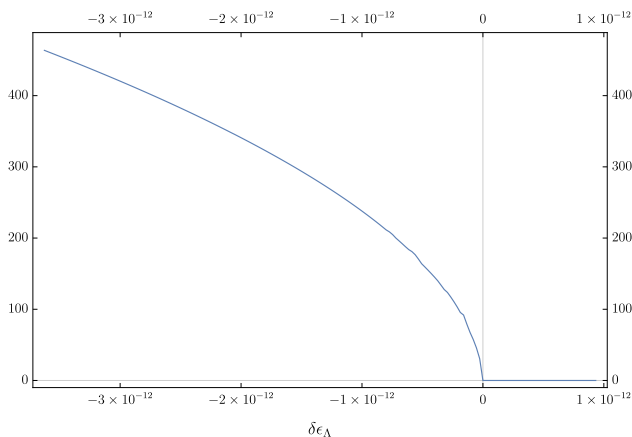


Figure 1. Second order quantum phase transition in the Higgs-top-bottom model [8]: the chiral order parameter (vacuum expectation value of the Higgs field)  $v$  is shown as a function of the control parameter  $\delta\epsilon_\Lambda$ . In the positive half plane we stay in the symmetric regime for the full flow, i.e. there is no vacuum expectation value  $v = 0$  in the long-range limit. For negative values of  $\delta\epsilon_\Lambda$ , we end up in the broken phase, as is indicated by a non-zero vev  $v$ . Near the critical point  $\delta\epsilon_\Lambda = 0$ , the increase of the order parameter is governed by a power law, Eq. (46), with critical exponent close to  $\beta \simeq 1/2$ . A physical value for the Fermi scale  $v \simeq 246$  GeV requires to fine-tune the control parameter rather closely to the phase transition.

Correspondingly, the model needs to be fine-tuned severely in order to achieve a large scale separation. For instance for Fig. 1, we have initiated the flow at  $\Lambda = 10^8$  GeV. In order to obtain a vacuum expectation value at the Fermi scale  $v \simeq 246$  GeV, we have to tune the control parameter to about  $\delta\epsilon_\Lambda \simeq -1 \times 10^{-12}$  in units of the cutoff  $\Lambda$ . A “natural choice” of  $\delta\epsilon_\Lambda \sim -\mathcal{O}(1)$  would have lead to a much larger order parameter and thus to unphysically large quark and Higgs masses near the cutoff scale. The required amount of fine tuning is governed by the critical exponent  $\Theta \simeq 2$ . Therefore, the naturalness problem could be reduced, if  $\Theta$  received large corrections to power-law scaling through a finite  $\eta$ .

The above reasoning is typically also applied to the

full standard model. This, however, relies on some assumptions, which might not be realized in nature. A first assumption is that the massless Gaussian fixed point be the relevant fixed point for the understanding of the properties of the system on all relevant scales. In presence of other fixed points with different properties, the sensitivity of the mass spectrum on bare parameters might be completely different. The second assumption is that – even at the Gaussian fixed point – the relevant operator related to a scalar bare mass parameter be the only/most significant deformation determining the mass spectrum of particles and in particular the physical value of the Higgs and W/Z bosons masses. In presence of more than one scale-breaking relevant deformation, this might not be the case. In particular, in asymptotically free non-Abelian gauge theories there is always one marginally-relevant deformation for each gauge coupling, with associated power-counting critical exponent  $\Theta = 0$ . The interplay of the chiral transition driving mechanisms and the understanding of the naturalness problem in presence of such couplings is however much less advanced, and at the heart of our following studies.

Upon inclusion of a QCD sector, the nature of the transition changes qualitatively rather independently of the initial conditions: as QCD is always in the chirally broken phase, the symmetric phase of the model disappears completely as does the critical point. The second-order quantum phase transition of the ungauged model is washed out and becomes a smooth crossover. Nevertheless, if the QCD scale is much smaller than the Fermi scale, we expect the comparatively sharp increase of the Yukawa model to remain a prominent feature of  $v$  as a function of  $\delta\epsilon_\Lambda$ . If this is the case, we refer to the large- $v$  regime to the left of this sharp increase as the *Higgs regime* in contradistinction to the *QCD regime* to the right of the rapid transition where  $v$  is much smaller.

If this is the case, we can still try to quantify this increase by a power-law scaling similar to Eq. (46) with a corresponding *pseudo-critical* exponent  $\beta$ . More precisely, we extract the pseudo-critical exponent of the chiral transition by fitting the vacuum expectation value in the Higgs regime to the power law ansatz (Eq. (46)). This procedure is illustrated in Fig. 2, where the chiral order parameter  $v$  (in arbitrary units) is plotted doubly-logarithmically as a function of the control parameter for different initializations of the gauge sector; here,  $\Delta g_\Lambda$  measures the deviation of the initial conditions for the gauge coupling from the physical point). Each case displays a clear power-law for the order-parameter scaling that can be fitted by Eq. (46).

In this way, we get an estimate for the pseudo-critical exponent  $\beta$ , even though the transition is actually a crossover. Using Eq. (51), we can re-express this exponent through  $\eta$ . Upon insertion of  $\eta$  into Eq. (50), we obtain a correction to scaling and can thus quantify the impact of the gauge sector on the amount of fine-tuning necessary to separate the Fermi scale from the UV scale  $\Lambda$ . If  $\eta$  is positive and sufficiently large, the naturalness

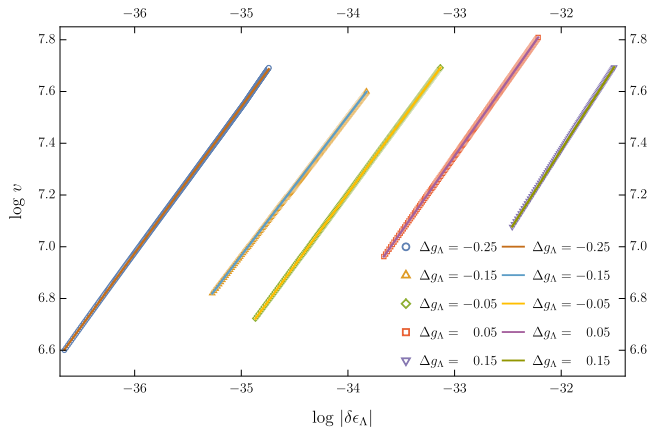


Figure 2. The phase transition of the full model in a logarithmic plot: the increase of the order parameter  $v$  (a.u.) is shown as a function of the control parameter  $\delta\epsilon_\Lambda$  in the regime of a strong increase of  $v$ , similarly to the left half plane of Fig. 1. The pseudo-critical exponent  $\beta$  for each choice of initial value of the gauge coupling can be extracted from the slope in this double-logarithmic plot (c.f. Eq. (46)).

problem of the model could be alleviated.

Let us finally point out two aspects that are not fully accounted for here: first, the  $SU(2)_L$  gauge group is ignored here but participates also as a potential source for chiral symmetry breaking in its strong-coupling regime. In the Higgs regime, this source is always screened by the finite gauge-boson masses. In the QCD regime, it is potentially active. However, since the QCD sector is much more strongly coupled, it dominates the chiral observables quantitatively. We expect our results to remain essentially unaffected, as long as we preserve the hierarchy of the two non-Abelian gauge sectors of the standard model.

Second, the picture of universality developed for the Higgs-top-bottom model is not exact since the model does presumably not feature a UV-complete limit. We therefore have to work with a finite UV cutoff  $\Lambda$ , implying that slight violations of universality can occur, but are generically suppressed by powers of  $1/\Lambda$ . We find that  $\Lambda = 10^8$  GeV is sufficient for our purposes. We have tested for violations of universality by varying the initial conditions of the marginal couplings on the  $\mathcal{O}(1)$  level. The residual non-universal effects in the QCD regime remain below the permille level, see App. E.

### A. The QCD regime

In the QCD regime, one expects the induced vacuum expectation value in the IR to be of the order of the scale of strong interactions  $\Lambda_{\text{QCD}}$ . In this work, we use a simple but useful definition of this scale by identifying it with the location of the IR Landau pole of the strong gauge coupling obtained from the one-loop beta

function. In the deep QCD regime, the phase transition is triggered by the gauge sector (more specifically via a strongly increasing four-fermion coupling in the effective action Eq. (3) before performing the partial bosonization), in contrast to quark and Higgs fluctuations in the deep Higgs regime. This corresponds to a choice of initial values where the scalar mass  $m^2 > 0$  is of the order of the UV scale  $\Lambda$ , making the scalar field non-dynamical and thus reducing our model to a low-energy effective theory of the strong interactions. In other words, a limiting case of our reduced standard model is the pure quark meson model [40], however with  $N_f = 6$  quark flavors.

The vacuum expectation value induced in the deep QCD regime depends solely on the value of the gauge coupling at the initialization scale  $g_\Lambda$ . Since there is no remnant of the electroweak Higgs mechanism in this regime, all quarks have zero current quark mass.

As it should be, the other marginal parameters of the model (scalar self-interactions and Yukawa couplings) have hardly any influence on the resulting vacuum expectation value. More precisely, their influence arises only because of the fact that we work with a finite UV cutoff  $\Lambda$ ; this introduces violations of universality which vanish exactly in the limit  $\Lambda \rightarrow \infty$ . For completeness, we quantify these universality violations in App. E for our practical choice  $\Lambda = 10^8$  GeV and find them to be on the sub-permille level for the quantities of interest.

This feature is expected since the gauge coupling  $g$  is the only parameter present in fundamental massless QCD. Through the scale anomaly encoded in the RG running manifesting in *dimensional transmutation*, it is linked to the dimensionful quantity  $\Lambda_{\text{QCD}}$  setting the scale for all long-range observables such as the vacuum expectation value  $v$ . The chiral condensate  $v$  and  $\Lambda_{\text{QCD}}$  are intimately connected; using our simple definition of  $\Lambda_{\text{QCD}}$  mentioned above, we list some quantitative results for varying initial values of the gauge coupling  $g_\Lambda$  in Tab. I. We see that while  $v$  and  $\Lambda_{\text{QCD}}$  vary a lot under shifts in  $g_\Lambda$ , the ratio of the two quantities stays approximately constant over ranges of the bare strong gauge coupling considered in this work. We consider the choice  $g_\Lambda = 0.719$  as the physical initial condition at  $\Lambda = 10^8$  GeV, since it corresponds to the experimentally measured value of  $\alpha_s(m_Z) = \frac{g^2(m_Z)}{4\pi} \simeq 0.117$  at the Z boson mass scale. This yields  $\Lambda_{\text{QCD}} \simeq 33$  MeV and  $v \simeq 2.1$  MeV for the IR QCD scales. Naively, this appears to be rather small compared to the physical values, e.g.  $v = f_\pi \simeq 93$  MeV. This, however, is a consequence of the fact that our IR flow proceeds with  $N_f = 6$  massless quarks down to the scale of symmetry breaking. Since the quarks induce screening, the gauge coupling grows strong at lower scales compared to the standard model case that includes the decoupling of the “heavy” quarks as a consequence of the Higgs mechanism.

Notice that the value of the chiral condensate  $v$  is consistently smaller than the scale obtained by the one-loop calculation. Both vary exponentially as a function of  $g_\Lambda$ . The results show that the ratio between the QCD

$g_\Lambda$	$\Lambda_{\text{QCD}}$ in GeV	$v_{\text{QCD}}$ in GeV	$v_{\text{QCD}}/\Lambda_{\text{QCD}}$
0.519	$6.4 \times 10^{-11}$	$4.8 \times 10^{-12}$	0.075
0.619	$1.6 \times 10^{-5}$	$1.1 \times 10^{-6}$	0.068
0.719	$3.3 \times 10^{-2}$	$2.1 \times 10^{-3}$	0.063
0.819	5.0	0.29	0.059
0.919	158	8.8	0.055
1.019	1911	101	0.053

Table I. Comparison of the QCD scale  $\Lambda_{\text{QCD}}$  (for simplicity defined by the location of the one-loop IR Landau pole for  $N_f = 6$  active quark flavors) and the vacuum expectation value in the deep QCD regime ( $v_{\text{QCD}}$ ). The *physical* initial condition  $g_\Lambda = 0.719$  is chosen at  $\Lambda = 10^8$  GeV such that we obtain the experimentally measured value of  $\alpha_s(m_Z) = \frac{g^2(m_Z)}{4\pi} = 0.117$  at the Z boson mass scale. The other bare couplings are set to zero at the high energy scale (scalar self interactions) or by IR physics (top and bottom Yukawa couplings). The chiral condensate however is (almost) independent of the values of these other couplings, as is checked in appendix E.

scale and the would-be-Fermi scale  $v$ , far from being a free parameter, actually features a maximum value of  $\mathcal{O}(10)$ . Furthermore we observe that the ratio of the two scales varies rather slowly over a wide range of initial conditions  $g_\Lambda$ .

## B. Pseudo-critical exponent

Let us now analyze the interplay between the chiral transitions in the full model. For this, we first choose initial values for the marginal couplings at the initialization scale  $\Lambda$ , and then vary the relevant parameter of the scalar potential, i.e. the control parameter  $\delta\epsilon_\Lambda$ . Integrating the flow equations yields the vacuum expectation value  $v$  as a function of  $\delta\epsilon_\Lambda$  similar to the chiral Higgs-top-bottom model, c.f. Fig. 1. As expected, the second order phase transition of the latter becomes a crossover for any finite value of the initial gauge coupling  $g_\Lambda$ , meaning that the discontinuity at  $\delta\epsilon_\Lambda = 0$  is smoothed in a neighbourhood of the would-be-critical point. The size of this critical region grows for increasing  $g_\Lambda$ , as illustrated in Fig. 3. Still, we generically observe a rather sharp transition between a Higgs-like and a QCD-like regime. In this regime, we identify the physical point for the Fermi scale where  $v = 246$  GeV. The required choice for the control parameter  $\delta\epsilon_\Lambda$  lies typically at small negative values; we call the deviation from this value  $\delta\epsilon_\Lambda^{\text{phys}}$ . Near the physical point, i.e. for  $|\delta\epsilon_\Lambda^{\text{phys}}| \ll 1$ , we fit the results for the vacuum expectation value to the scaling hypothesis coming from the theory of second order phase transitions, that is Eq. (46). Example results of such fits have been shown in Fig. 2. Deviations from canonical power-counting scaling occurs as departures of the pseudo-critical exponent  $\beta$  from the value  $\beta = 1/2$ , which we measure in terms of the pseudo-critical correction-to-scaling ex-

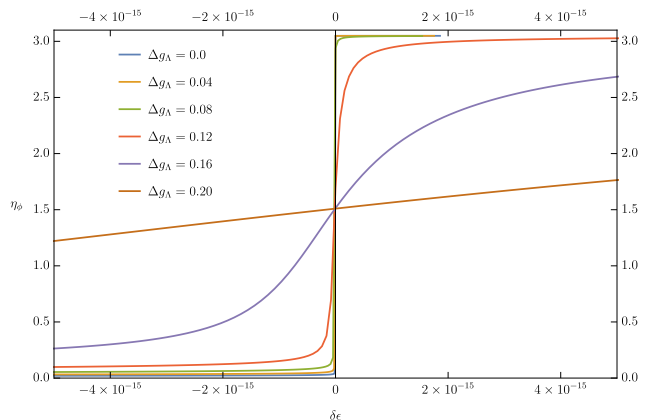


Figure 3. The scalar anomalous dimension  $\eta_\phi$  at the transition scale. A small  $\eta_\phi$  corresponds to a Higgs-like regime ( $\delta\epsilon < 0$ ) whereas a large one can be identified with a QCD-like regime. While for small gauge couplings  $g_\Lambda$  the scalar anomalous dimension jumps at the critical point (characterized by  $\delta\epsilon = 0$ ), indicating that a critical point for a second order phase transition can be straightforwardly defined, and thus extracting a pseudo-critical exponent is sensible. For large gauge couplings, this region grows, making it hard to define a critical point as well as extract a meaningful pseudo-critical exponent.

ponent  $\eta$  according to Eq. (51). As discussed above, finite positive values of  $\eta$  are a direct quantitative measure of how the interplay of the chiral transitions in the standard model alleviates the naturalness problem.

Let us investigate how this quantity depends on the microscopic parameters of the Lagrangian at the scale  $\Lambda$ . In general, changing a microscopic parameter changes the physical quantities of the theory. For instance, changing the top-Yukawa coupling in the Higgs regime corresponds to changing the top mass relative to the vacuum expectation value. However, this direct influence on the long-range observables becomes less pronounced – and even vanishes ultimately – in the deep QCD regime where the full model is dominated by the gauge sector. Since the physical point is near the transition from the Higgs to the QCD regime, the precise dependence of the pseudo-critical exponent on the microscopic couplings is a priori unclear.

The computational procedure is the same for all parameters of interest: we keep all couplings fixed at the initialization scale  $\Lambda$  while varying the control parameter  $\delta\epsilon_\Lambda^{\text{phys}}$  to extract the behavior of the phase transition and to measure  $\eta$  for a given set of parameters. We repeat this for different values of the coupling of interest at  $\Lambda$ , while keeping all other values fixed. Results are shown in Fig. 4 for all couplings in the model except for the gauge coupling. We find that the pseudo-critical exponent  $\eta$  remains basically unaffected by the initial value of the Yukawa and scalar couplings in the explored regime. The data in Fig. 4 shows only some glitches on top of a constant value which reflect the numerical pre-

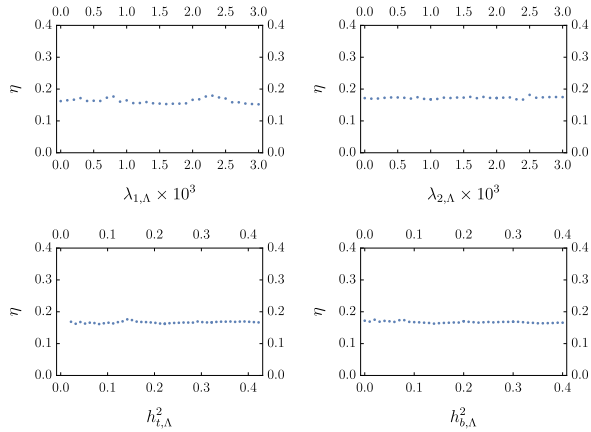


Figure 4. The critical exponent  $\eta$  for different couplings at the high energy scale  $\Lambda$ : the quartic couplings  $\lambda_1$  (upper left panel) and  $\lambda_2$  (upper right), and the Yukawa couplings of the top (lower left) and bottom (lower right) quarks. The gauge coupling  $g_\Lambda$  at the initialization scale is kept fixed at the physical value. The size of the fluctuations of  $\eta$  is a measure for the numerical precision.

cision. The fine-tuning procedure necessary to arrive at  $v = 246$  GeV together with the large integration range starting from  $\Lambda = 10^8$  GeV leaves room for an accumulation of numerical errors. For practical reasons, we have restricted the scalar couplings to relatively small values, since stronger scalar self-interactions would require the flow to already start in the broken regime. This choice is also justified by the observation that the Higgs quartic coupling in the full standard model appears to be nearly vanishing at the Planck scale.

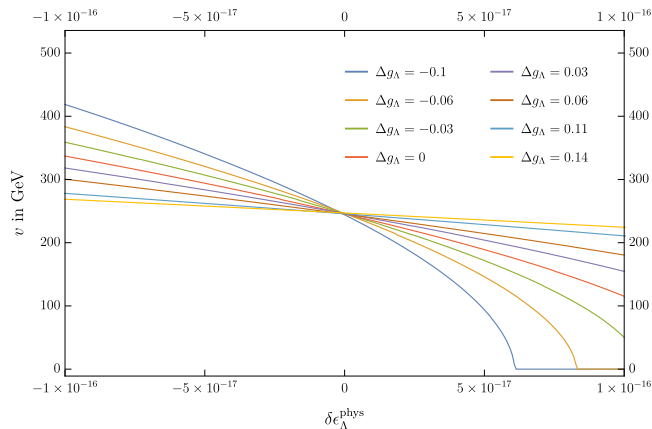


Figure 5. Vacuum expectation value in vicinity of the Fermi scale  $v = 246$  GeV for different values of the gauge coupling  $g_\Lambda$  at the UV scale. For larger gauge couplings we observe less change in the vacuum expectation value under variation of the relevant direction of the scalar potential at the high energy scale  $\delta\epsilon_\Lambda$ , indicating a stronger interplay of the phase transitions and a corresponding mitigation of the naturalness problem.

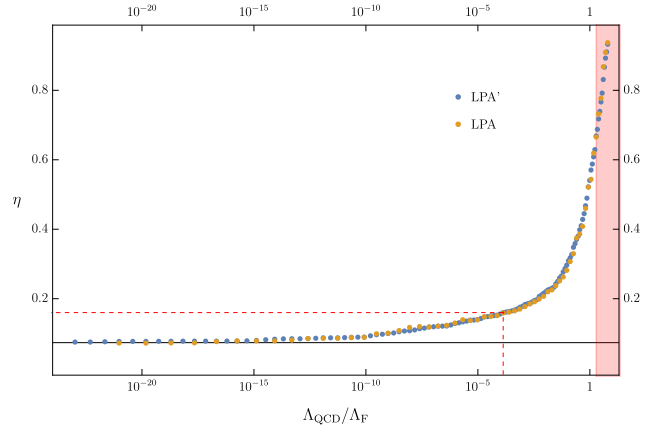


Figure 6. Pseudo-critical exponent  $\eta$  for different initial conditions of  $g_\Lambda$ . By dimensional transmutation, we express  $g_\Lambda$  as the QCD scale  $\Lambda_{\text{QCD}}$  (for  $N_f = 6$ ). The Fermi scale  $\Lambda_F$  is fixed to 246 GeV for this work. The interplay between the chiral transitions in the standard model becomes the more pronounced the closer the two scales are. For  $\Lambda_{\text{QCD}} \rightarrow \Lambda_F$ , the naturalness problem weakens significantly. The physical point corresponding to a standard-model-like running of the gauge coupling is denoted by the red dotted line. The shaded region on the right marks the regime where the chiral transition gets so smooth that the pseudo-critical exponent becomes less meaningful.

By contrast, varying the initial value of the gauge coupling has a strong influence on the transition from the Higgs to the QCD regime. This is visible in Fig. 5, where the slope of the order parameter field  $v$  as a function of the control parameter flattens for increasing values of the gauge coupling; the latter is expressed in terms of the deviation  $\Delta g_\Lambda$  of the initial condition from the physical point. This has a direct impact on the naturalness problem: the flatter the curve is when it crosses the physical point, the less fine-tuning is needed to put the system in the vicinity of the Fermi scale. We emphasize that the physical point  $\Delta g_\Lambda = 0$  already exhibits a flatter curve than the pure Higgs-top-bottom model with canonical power-counting. This demonstrates that the QCD sector in the standard model already alleviates the naturalness problem compared to a pure Higgs-Yukawa model which is often used to illustrate the naturalness problem.

Quantifying these results analogously to the previous analysis, we again extract the pseudo-critical exponent  $\eta$  for these transitions. The interplay of the chiral transitions and the alleviation of the naturalness problem is visible from the monotonic increase of  $\eta$  as a function of  $g_\Lambda$ . In Fig. 6, we plot the corresponding critical exponent against the dimensionless ratio  $\Lambda_{\text{QCD}}/\Lambda_F$ ; here, we have translated  $g_\Lambda$  into  $\Lambda_{\text{QCD}}$ , denoting the QCD scale coming from dimensional transmutation,  $\Lambda_F$  denotes the Fermi scale which is set to 246 GeV for this work.

Deep inside the Higgs regime, i.e. for  $\Lambda_{\text{QCD}}/\Lambda_F \rightarrow 0$ ,

we observe that the pseudo-critical exponent approaches a constant value  $\eta \simeq 0.07$ . This is the value of the pure Higgs-top-bottom model arising from the fluctuations in the Yukawa sector. Surprisingly, already in the limit of negligible QCD corrections, the critical exponent differs from the pure Gaussian value. This is an effect of having fixed the IR observables, such as the Fermi scale  $v$  and the top mass  $m_t^2$ , a requirement that forces the theory off the Gaussian fixed point. A more explicit argument supporting this interpretation is presented in the next section.

For an increasing scale ratio  $\Lambda_{\text{QCD}}/\Lambda_{\text{F}}$  also  $\eta$  increases, exemplifying a stronger interplay of the chiral transitions. At the physical point which in our definition is characterized by  $\Lambda_{\text{QCD}} = 33$  MeV, we observe that the pseudo-critical exponent takes the value  $\eta = 0.16$ . We take this as a manifestation that the QCD sector exerts a non-negligible influence on the chiral transition. Quantitatively, the naturalness problem of the standard model is mildly alleviated by this interplay, even though the reduction of the power-law scaling from the canonical value  $\Theta = 2$  to  $\Theta \simeq 1.84$  remains on the 10% level and thus does not make a qualitative difference.

A “solution” of the naturalness problem would require a pseudo-critical exponent  $\eta \sim \mathcal{O}(1)$ . For values of  $\Lambda_{\text{QCD}}$  larger than the physical point, we observe the onset of a strong increase of  $\eta$  near  $\Lambda_{\text{QCD}}/\Lambda_{\text{F}} \simeq 10^{-2}$ . Physically this implies that an increasing part of the chiral order parameter is generated by the QCD sector. Correspondingly, the separation of  $v$  from the cut-off scale  $\Lambda$  requires less and less fine-tuning of the bare parameters in the Higgs sector, but is taken care of by chiral symmetry breaking of QCD. The scale of the latter depends only logarithmically on the high scale and a large scale separation thus becomes natural.

However recall that the ratio  $\Lambda_{\text{QCD}}/\Lambda_{\text{F}}$  cannot attain arbitrarily large values, as we argued in the previous section. Furthermore, the simplistic description of Fig. 5 of chiral-symmetry breaking in terms of a pseudo-critical exponent  $\eta$  breaks down well below that upper bound. This is because the behavior of  $v$  across the transition between the symmetric and the SSB regime ceases to be comparable to the power-law ansatz of Eq. (46) for too large  $g_\Lambda$ ; in Fig. 6 this is indicated by the shaded region.

### C. Scaling behaviour near the QCD-dominated regime

As observed in the preceding section, the pseudo-critical exponent exhibits a strong increase beyond  $\Lambda_{\text{QCD}}/\Lambda_{\text{F}} \gtrsim 10^{-2}$ . We argue in the following that this can be understood within a simple approximation of the flow equations. Approaching the QCD regime from the side of the Higgs regime, the RG flow transition between the symmetric and SSB regimes starts to occur closer and closer to  $\Lambda_{\text{QCD}}$ . Near the latter, the running of the Yukawa coupling, as well as the scalar self interaction,

becomes governed by the flow of the strong gauge coupling  $g^2$ . This can be seen by looking at the  $\beta$  functions of these couplings in a specific limit:

Right above the scales before the RG flow enters the SSB regime, the dimensionless mass parameter  $\epsilon$ , and thus the scalar masses, are negligible; by contrast, the meson Yukawa coupling  $h^2$  near the QCD regime is much larger than the top and bottom Yukawa couplings, which therefore can be set to zero for the present analysis. Looking at the flow equations in this limit reveals that there are quasi fixed points in the composite couplings  $h^2/g^2$  and  $\lambda_1/h^2$ , implying that the evolution of  $h^2$  and  $\lambda_1$  are directly connected to the flow of  $g^2$ . This kind of partial fixed point behavior is well known both as a feature of IR flows, in which case it is called a Pendleton-Ross kind of fixed point [89], as well as a UV signature of total asymptotic freedom or safety, in which case it has been referred to with a variety of names: eigenvalue condition [90, 91], reduction of couplings [92, 93], nullcline [94], fixed flow [95] or quasi fixed point [96, 97]. In the present model, the quasi fixed point as a solution of the RG equations has been first described by Cheng, Eichten and Li (CEL) [98], and we therefore call it a CEL solution.

In this specific limit and considering for simplicity the one-loop approximation for all beta functions of interest here, we have

$$\begin{aligned} \partial_t g^2 &= -\frac{7}{8\pi^2} g^4, \\ \partial_t h^2 &= \frac{h^2}{16\pi^2} \left( \frac{19}{2} h^2 - 16g^2 - 12\frac{g^4}{h^2} \right), \\ \partial_t \lambda_1 &= \frac{\lambda_1}{4\pi^2} \left( 3h^2 + 4\lambda_1 - \frac{3}{2} \frac{h^4}{\lambda_1} \right). \end{aligned} \quad (52)$$

Note that the last terms of the flow of  $h$  and  $\lambda_1$  arise from dynamical bosonization. In Eq. (52), we have already set  $d = 4$ ,  $N_f = 2$  in the Higgs-top-bottom sector beta functions,  $N_f = 6$  for the gauge coupling, and  $N_c = 3$ . It is useful to introduce rescaled couplings  $\hat{h} = \frac{h}{g}$ , as well as  $\hat{\lambda}_1 = \frac{\lambda_1}{h^2}$ . Their flow equations read

$$\begin{aligned} \partial_t \hat{h}^2 &= \frac{1}{32\pi^2} g^2 \left( 19\hat{h}^4 - 4\hat{h}^2 - 24 \right), \\ \partial_t \hat{\lambda}_1 &= \frac{1}{32\pi^2} \frac{g^2}{\hat{h}^2} \left[ 24\hat{\lambda}_1 + 32\hat{h}^2 \hat{\lambda}_1 \right. \\ &\quad \left. + \hat{h}^4 \left( 32\hat{\lambda}_1^2 + 5\hat{\lambda}_1 - 12 \right) \right], \end{aligned} \quad (53)$$

each of which exhibit a fixed point. These fixed points imply that we have  $h^2 \sim g^2$  and  $\lambda_1 \sim h^2 \sim g^2$  within the validity regime of these one-loop equations. Correspondingly, the scalar anomalous dimension takes the form

$$\eta_\phi = \frac{3}{8\pi^2} h^2. \quad (54)$$

As a consequence, in an intermediate interval of values of  $g_\Lambda$ , where the latter grows but the system is not yet

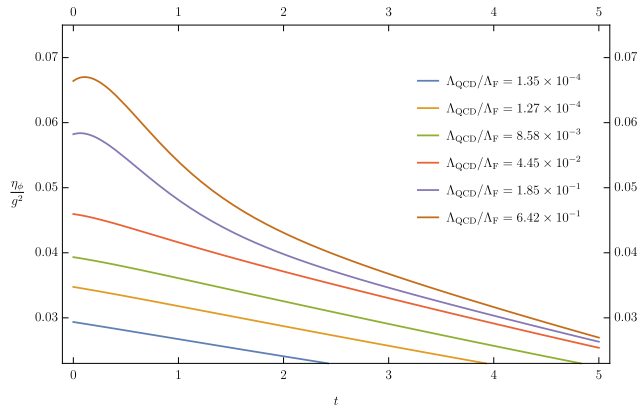


Figure 7. The running of  $\eta_\phi/g^2$  close to the transition from the disordered to the ordered phase for different scale separations  $\Lambda_{\text{QCD}}/\Lambda_{\text{F}}$ . The RG time  $t$  is normalized such that  $t = 0$  coincides with the transition scale. We can see that for increasing values of  $g_\Lambda$ , and thus  $\Lambda_{\text{QCD}}/\Lambda_{\text{F}} \rightarrow 1$ , the running of  $\eta_\phi/g^2$  levels out, corresponding to the quasi fixed-point in  $\hat{h}$  and  $\hat{\lambda}$ .

fully dominated by QCD fluctuations, the scalar anomalous dimension scales as  $g^2$  close to the transition. This can be seen in Figure 7, where the flattening of the three upper trajectories near  $t = 0$  (the RG time at which the flows enter into the SSB regime) signals an effective scaling  $\eta_\phi \sim g^2$ . When this happens, the quasi-fixed point value of the field anomalous dimension at the transition in turn becomes a good approximation of the pseudo-critical exponent, as we now argue.

This phenomenon can be qualitatively understood as a manifestation of the fact that a strongly growing scalar anomalous dimension has a sizable impact on the running of the (dimensionless) mass parameter of the scalar potential:

$$\partial_t \epsilon = -(2 - \eta_\phi)\epsilon - \frac{5}{8\pi^2}\lambda_1 + \frac{3}{8\pi^2}h^2. \quad (55)$$

An increasing and large value of  $\eta_\phi$  modifies the canonical quadratic running of  $\epsilon$  substantially and eventually removes the fine-tuning problem, as is expected in a QCD-dominated model. At the transition from the unbroken to the broken phase, the scalar anomalous dimension can therefore be expected to be related to the critical exponent  $\eta$ . This is highlighted and quantitatively confirmed by a comparison of the value of the scalar anomalous dimension  $\eta_\phi$  (computed within the full set of flow equations) at the SYM-SSB transition scale, and the pseudo-critical exponent  $\eta$  obtained from the power law behavior of the vacuum expectation value  $v$  close to the critical point (c.f. Eq. (46)), which is shown in Fig. 8.

Starting from the deep Higgs regime for very low ratio  $\Lambda_{\text{QCD}}/\Lambda_{\text{F}}$ , one can see in this figure that the anomalous dimension at the transition scale is positive  $\eta_\phi > 0$  already in the pure Higgs-top-bottom model, since a nonvanishing top Yukawa coupling is required by the

IR conditions imposed on the RG trajectories. In this limit, we observe that  $\eta$  is bigger than  $\eta_\phi$  at the transition by about an order of magnitude. We attribute this to a built-up of fluctuations at the onset of the SSB regime from the transition scale to the freeze out scale. This is a nontrivial result stemming from the threshold and strong coupling effects along the RG flows. On the other hand, moving towards the intermediate region, both quantities exhibit a strong increase and approach each other towards values of  $\eta \sim \mathcal{O}(1)$  near  $\Lambda_{\text{QCD}}/\Lambda_{\text{F}} \simeq 10^{-1}$ ; the latter correspond to  $g_\Lambda$  values that trigger the onset of the quasi-fixed-point behavior at the transition.

As a final remark on this intermediate scaling behavior, let us mention another line of reasoning that can be used to qualitatively expect and understand the results presented above. Since the region between the deep Higgs and the deep QCD regimes corresponds to intermediate values of the mass parameter  $\delta\epsilon$ , it can be expected to include an almost-critical point of minimal breaking of scale invariance. The latter is in fact explicitly and severely broken in the two opposite extrema of a deep Mexican-hat standard-model-like Higgs potential ( $\delta\epsilon \ll -1$ ) and of a very massive quasi-decoupled QCD-like meson ( $\delta\epsilon \gg 1$ ). Scale invariance is a defining property of RG fixed points. In the present model the only complete fixed point featured by our RG equations is the Gaussian one. The CEL solution in turn describes the UV critical surface of this fixed point in its vicinity, that is, the weak-coupling parameterization of the locus of points corresponding to a minimal breaking of scale invariance. In fact, the relevant, i.e. mass-like, deformation from the fixed point is zero on this surface. Hence, in the weakly coupled perturbative regime, the CEL solution describes a technically natural theory, where the Higgs mass needs no fine tuning and stays small due to the approximate scale symmetry, which is broken only dynamically by QCD through a Coleman-Weinberg mechanism. This expectation must be confronted with the necessity to exit the mere perturbative regime and follow the theory at strong coupling in the IR. The results of this section therefore can be interpreted as a first quantitative test of this perturbative understanding, beyond the weakly coupled regime. Surprisingly, the CEL solution appears to provide a fair first approximation of the location of the “natural” theory in the phase space of the model, even if for  $\Lambda = 10^8$  GeV the latter is close to  $g_\Lambda^2 = \mathcal{O}(1)$ .

Let us stress that the precise value of  $\eta$  at the physical point in Fig. 8 is not only determined by the IR value of measured quantities, but also depends on theoretical assumptions, such as the precise RG flow of the standard model. Shifting the  $\eta$  curve along the  $\Lambda_{\text{QCD}}/\Lambda_{\text{F}} \simeq 10^{-2}$  axis is possible by changing the RG evolution, thus effectively changing  $g_\Lambda$ , while keeping the IR parameters fixed. Determining the RG flow is not only a matter of improving the approximations over the nonperturbative domain of the theory, but also and primarily a question of *defining* the quantum field theory beyond perturba-

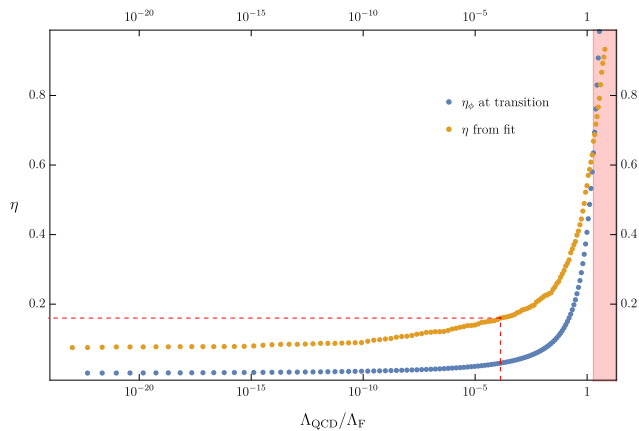


Figure 8. Comparison of the pseudo-critical exponent  $\eta$  and the scalar anomalous dimensions  $\eta_\phi$  evaluated near the transition of the RG flow from the symmetric to the broken regime using the full set of flow equations. Both exhibit a strong increase towards values of  $\mathcal{O}(1)$  near  $\Lambda_{\text{QCD}}/\Lambda_{\text{F}} \simeq 10^{-2}$  indicating a strong interplay of the chiral transitions. The physical point, characterized by the running of the gauge coupling, is denoted by the red dashed line.

tion theory. As a possible embodiment of this fact we can refer to the scenario of Ref. [99, 100] where new solutions of the RG equations were constructed by appropriately parametrizing the boundary conditions on the scale-dependent effective action. These generalized solutions and the new parameters that they involve allow to vary the RG flow between the UV scale  $\Lambda$  and the IR, while preserving the observables at the latter scale.

#### D. Electroweak Gauge Bosons

So far, we have ignored the electroweak gauge sector, as it contributes only subdominantly to the interplay of the chiral transitions. In turn, however, the chiral transition, of course, affects the electroweak gauge sector strongly. This is well known and fully standard in the Higgs regime, where the chiral transition at the same time features the BEH mechanism, rendering part of the electroweak gauge bosons massive. But analogous results also hold in the QCD regime. In other words, the BEH mechanism does not need to be triggered by a carefully designed or even fine-tuned scalar potential, but is also operative if the vacuum expectation value of a composite effective scalar field is generated by other interactions, such as the QCD sector.

As an illustration, let us include ingredients of the electroweak gauge sector on an elementary level in order to estimate the mass of the electroweak gauge bosons as a consequence of the chiral transition in the QCD regime.

For this, we use the flow equations extracted for the model (c.f. Sect. III), and amend them with the one-loop flow equation obtained for the SU(2) gauge cou-

pling  $g_{\text{EW}}$ .

$$\partial_t g_{\text{EW}} = -\frac{g_{\text{EW}}^3}{(4\pi)^2} \left( \frac{22}{3} - \frac{4}{3} n_g - \frac{1}{6} \right). \quad (56)$$

The first term in the parenthesis comes from gauge boson loops, the second one from fermionic loops and the last contribution stems from scalar loops. Since in our analysis we focus on flows which start in the symmetric regime and end up in the broken one, no threshold functions accounting for the masses of the degrees of freedom are necessary for the gauge and fermionic loops in the symmetric regime. The scalar field however is massive in the SYM regime, and in this regime we will account for this effect by introducing the mass threshold corresponding to two internal scalar propagators of the Higgs field for this contribution,

$$-\frac{1}{6} \rightarrow -\frac{1}{6} \frac{1 - \frac{\eta_\phi}{6}}{(1 + \epsilon)^2}. \quad (57)$$

This coincides with the standard perturbative contribution in the deep euclidean region  $\epsilon \rightarrow 0$ . In the following, we ignore the hypercharge sector and thus also the mass splitting of the  $W$  and  $Z$  bosons.

As soon as the flow enters the broken regime, the gauge bosons and fermions obtain masses, leading to a freeze-out of the flow in this regime. As a simple approximation, we use the value of the electroweak gauge coupling at the transition scale as the relevant IR value for an estimate of the  $W$ -boson mass.

The  $W$  mass can then be read off straightforwardly, since it is fully determined by the vacuum expectation value  $v$  and the freeze-out value of its gauge coupling  $g_{\text{EW,IR}}$  through

$$m_W = \frac{1}{2} g_{\text{EW,IR}} v. \quad (58)$$

The initial conditions for the flow of the electroweak gauge coupling are chosen such that they coincide with the running in the standard model, namely its value at the  $Z$  boson mass scale,

$$\frac{g_{\text{EW}}^2}{4\pi} (M_Z) \simeq 0.034, \quad \text{where } M_Z = 90.117 \text{ GeV}. \quad (59)$$

In Fig. 9, we depict the resulting mass values for the  $W$  boson across the chiral transition region for various initial values of the QCD gauge coupling. In the Higgs regime, we observe the conventional strong dependence of the gauge boson mass on the control parameter which needs to be fine-tuned to obtain the Fermi scale and – as a consequence – the physical value of the  $W$  boson mass. For any nonvanishing value of the QCD gauge coupling, the transition is actually a crossover, such that the vacuum expectation value as well as the  $W$  boson mass never vanish. In fact, in the deep QCD regime, both dimensionful quantities approach a non-zero value which is dominated by the QCD sector.

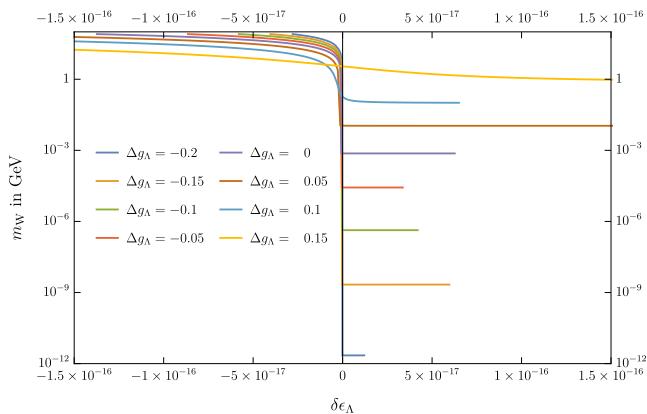


Figure 9.  $W$  boson mass for different initial values of the strong gauge coupling at the UV scale  $g_\Lambda$  as a function of the initial (dimensionless) mass parameter  $\delta\epsilon_\Lambda$ . Because the gauged system features only a crossover, the  $W$  boson mass is nowhere zero in the phase diagram. Instead, we observe a lower bound for the  $W$  boson mass in the QCD regime (corresponding to  $\delta\epsilon_\Lambda \gg 0$ ).

In this regime, the scale is set purely by the gauge coupling, or (after dimensional transmutation) by  $\Lambda_{\text{QCD}}$ . In order to illustrate this dependence, we plot the resulting plateau value for the  $W$  boson mass as a function of the QCD induced chiral condensate  $v = v_{\text{QCD}}$ , see Fig. 10. We observe an essentially linear dependence. This plateau value can be interpreted as the minimum possible value of the  $W$  boson mass for the case that the BEH mechanism is not driven by a scalar Higgs potential but fully by the chiral QCD transition. This minimum  $W$  boson mass value has, for instance, been estimated in [14, 15]. However, a comparison of differ-

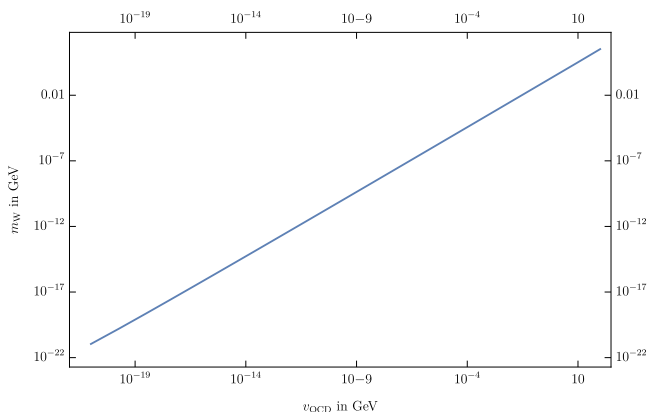


Figure 10. The minimal  $W$  boson mass in the deep QCD regime for different values of  $g_\Lambda$ , expressed through the chiral condensate  $v_{\text{QCD}}$ . We extract the mass of the weak vector bosons in the far right half plane of Fig. 9 and plot it against the chiral vev obtained in the QCD regime. We observe an essentially linear dependence of the mass on the QCD-induced vacuum expectation value.

ent results is inflicted by the fact that it involves not only a comparison of approximations within a theory, but rather a comparison of different theories that arise from fixing quantum field theories differently at different scales.

Taking our approach at face value, the scale in the QCD regime is set by fixing the gauge coupling to its physical value at a high scale, before evolving it into the IR. As discussed above, this leads to a rather small value of the chiral condensate  $v \simeq 2.1$  MeV in the QCD regime as a consequence of the fact that the QCD sector runs with  $N_f = 6$  (screening) massless flavors all the way down to the SSB regime. As a consequence, our straightforward estimate of the minimum  $W$  boson mass value is  $m_W = 0.74$  MeV, which is a rather small value compared to other estimates.

However, instead of matching our parameters to those of the physical standard model at the high scale, we could also perform a low scale matching: one possible choice (among many others) is to fix the couplings such that the chiral condensate acquires its physical value  $v = f_\pi \simeq 93$  MeV also in the deep QCD regime. As a consequence, our prediction for the  $W$  boson mass would be  $m_W = 33$  MeV which is similar to that of [14].

## V. CONCLUSIONS

The naturalness puzzles of the standard model, e.g. the gauge or the flavor hierarchy problems or the strong CP problem, are typically addressed within pure model-building arenas. In this sense, a common attitude is the expectation that "solving" these problems amounts to creatively devising new models able to draw a simple straightforward prediction of parameters that would remain otherwise free and mysterious within the standard model. It is fair to say that this goal often remains unattained, unfortunately. Several popular and largely appreciated proposals for beyond-the-standard-model physics, such as for instance technicolor or axions, actually require complex nonperturbative computations to extract quantitative predictions.

Even within the standard model itself, it is difficult to quantitatively assess how *unnatural* the measured value of some key parameter is; in general, this requires quite nontrivial computations which go beyond the weakly-coupled perturbative regime. This problem is intrinsic in the way in which naturalness questions are often posed, that relies on the ability to connect the input values at some microscopic UV scale to the output values extracted from experiments. The larger the gap between these two scales, the harder the computations. In the standard model, the main responsible building block for this difficulty is the QCD subsector: the IR fluctuations of gluons are not tamed by any BEH mechanism, contrary to the electroweak  $W/Z$  bosons, and their interactions grow stronger at lower energies.

The task of properly defining and quantifying *unnaturalness* is further aggravated by the ambiguity in the

choice of the UV scale at which the microscopic parameters ultimately determining the measured observables are fixed. This second problem is caused by the fact that the standard model – as we understand it – is not a UV complete theory. The main troublemaker in this case is the electroweak sector, and specifically the  $U(1)_Y$  gauge coupling. Finally, there is a priori no preferred probability distribution for the microscopic parameters with respect to which naturalness can be quantified; also in this work, we implicitly use a flat distribution as is standard for the discussion of tuning a control parameter to a (quantum) phase transition.

In the present work, we have focused on the gauge-hierarchy problem as a prototypical naturalness case study. We have explored the possibility to quantitatively describe this feature of the standard model, by adopting modern techniques inspired by effective field theories and the renormalization group, while pushing them into the nonperturbative territory.

In this manner, we have been able to study the interplay of the two main sources of chiral symmetry breaking of the standard model: the electroweak Higgs interactions and the QCD sector. Whereas the breaking scales, i.e., the Fermi and the QCD scale, are several orders of magnitude apart, we observe a qualitative and quantitative interplay: the second-order transition of a pure Higgs-top-bottom sector is turned into a crossover by the presence of the QCD sector, see Fig. 3. We suggest to quantitatively characterize the deviation from Gaussianity of the Higgs-mass fine-tuning problem by means of a pseudo-critical exponent  $\eta$ . A result of this study is that the QCD sector alleviates the naturalness problem naively quantified by the quadratic running of the Higgs mass parameter by a pseudo-critical exponent  $\eta$  on the order of  $\sim 10\%$ , see Fig. 4. Remarkably, we have observed that  $\eta$  is nonvanishing even in case of negligible QCD corrections.

These conclusions have been drawn within the usual understanding of the standard model as an effective theory below a suitable UV cutoff, which in our study was set at  $\Lambda \sim 10^8$  GeV, and with bare couplings at this scale fully in the perturbative regime. The only non-standard ingredient we used in our investigation is a non-perturbative improvement of the RG equations to capture threshold effects in the matter sector and the expected strong-coupling regime of the QCD gauge coupling.

As a useful ingredient of our analysis, we have managed to describe the fundamental Higgs field and a mesonic composite scalar field on the same footing. This is particularly insightful for the study of deformations of the standard model in which the Fermi and the QCD scale are shifted relative to each other. Specifically, an increase of the QCD scale demonstrates that the standard model can be continuously connected to a deformed model where all scales are set by the QCD sector and the pseudo-critical exponent renders the connection between microscopic and macroscopic parameters natural.

In the latter case, the theory appears to enter into an

almost scale invariant regime which lies in a narrow intermediate window between the deep Higgs and the deep QCD regimes. This pseudo-critical region, where mass is expected to be generated by a Coleman-Weinberg mechanism, has been shown to be well approximated by a quasi-fixed point condition of the Cheng-Eichten-Li type [98], despite the fact that for standard-model-like IR observables this happens to require values of the bare gauge coupling  $g_\Lambda$  of order one.

This observation motivates interest in applying similar methods to investigate the naturalness problem of extensions of the standard model which are able to render the Coleman-Weinberg scenario compatible with the measured values of IR observables. Among these, of particular interest are UV complete extensions, since in these models the quasi-fixed-point behavior is expected to be continuously connected with the controlled UV asymptotics for increasing values of  $\Lambda$ .

Of course, our treatment of the nonperturbative QCD sector is rather rudimentary and relies on some model input in the pure gauge sector. Nevertheless, it is capable of connecting the microscopic description in terms of quarks and gluons to a long-range description on terms of a quark-meson model that can be matched quantitatively to chiral perturbation theory. Still, there is, of course, room for substantial improvement required for claiming a full quantitative control of the nonperturbative domain. For instance, in the deep QCD regime we have estimated the radiatively generated mass of the W boson. We expect this estimate to be inflicted by the approximations and assumptions made in this nonperturbative sector. Another subtle issue that we have not investigated in this work, is the possible gauge and parametrization dependence of our results, which we leave for future developments.

Nevertheless, we believe that our approach offers a useful framework for addressing the interplay of the chiral transitions in the standard model. As the transitions are considered to root in rather different sectors, such a treatment in a unified framework is valuable and has been missing so far.

## ACKNOWLEDGMENTS

We are grateful to Axel Maas, Daniel Litim, Roberto Percacci, Simon Schreyer, René Sondenheimer, Jan Pawłowski, Gian Paolo Vacca, and Christof Wetterich for helpful discussions. This work has been funded by the Deutsche Forschungsgemeinschaft (DFG) under Grant Nos. 398579334 (Gi328/9-1) and 406116891 within the Research Training Group RTG 2522/1. This project has also received funding from the European Union’s Horizon 2020 research and innovation programme under the Marie Skłodowska-Curie Grant Agreement No. 754496.

### Appendix A: Flow equations of the model

The flow equations of the model are derived using the functional renormalization group flow equation for the effective action 32. Here all results are expressed in terms of dimensionless quantities, c.f. Eq. (34).

For the Yukawa couplings we obtain

---


$$\begin{aligned}
\partial_t h^2 = & \left( d - 4 + \eta_b + \eta_t + \eta_{\tilde{\phi}} \right) h^2 + v_d h^4 \left\{ l_{1,1}^{(\text{FB})d} \left( \mu_t^2, \mu_m^2; \eta_t, \eta_{\tilde{\phi}} \right) + l_{1,1}^{(\text{FB})d} \left( \mu_b^2, \mu_m^2; \eta_b, \eta_{\tilde{\phi}} \right) + l_{1,1}^{(\text{FB})d} \left( \mu_t^2, \mu_{m,r}^2; \eta_t, \eta_{\tilde{\phi}} \right) \right. \\
& + l_{1,1}^{(\text{FB})d} \left( \mu_b^2, \mu_{m,r}^2; \eta_b, \eta_{\tilde{\phi}} \right) + l_{1,1}^{(\text{FB})d} \left( \mu_t^2, \mu_m^2; \eta_t, \eta_{\tilde{\phi}} \right) + l_{1,1}^{(\text{FB})d} \left( \mu_b^2, \mu_m^2; \eta_b, \eta_{\tilde{\phi}} \right) + l_{1,1}^{(\text{FB})d} \left( \mu_t^2, \mu_m^2; \eta_t, \eta_{\tilde{\phi}} \right) \\
& + l_{1,1}^{(\text{FB})d} \left( \mu_b^2, \mu_m^2; \eta_b, \eta_{\tilde{\phi}} \right) + l_{1,1}^{(\text{FB})d} \left( \mu_t^2, \mu_G^2; \eta_t, \eta_{\tilde{\phi}} \right) + l_{1,1}^{(\text{FB})d} \left( \mu_t^2, \mu_H^2; \eta_t, \eta_{\tilde{\phi}} \right) + l_{1,1}^{(\text{FB})d} \left( \mu_t^2, \mu_G^2; \eta_t, \eta_{\tilde{\phi}} \right) \\
& + l_{1,1}^{(\text{FB})d} \left( \mu_t^2, \mu_G^2; \eta_t, \eta_{\tilde{\phi}} \right) + l_{1,1}^{(\text{FB})d} \left( \mu_b^2, \mu_G^2; \eta_b, \eta_{\tilde{\phi}} \right) + l_{1,1}^{(\text{FB})d} \left( \mu_b^2, \mu_H^2; \eta_b, \eta_{\tilde{\phi}} \right) + l_{1,1}^{(\text{FB})d} \left( \mu_b^2, \mu_G^2; \eta_b, \eta_{\tilde{\phi}} \right) \\
& \left. + l_{1,1}^{(\text{FB})d} \left( \mu_b^2, \mu_G^2; \eta_b, \eta_{\tilde{\phi}} \right) \right\} - 4(3 + \xi) \frac{N_c^2 - 1}{2N_c} g^2 h^2 \left\{ l_{1,1}^{(\text{FB})d} \left( \mu_t^2, 0; \eta_t, \eta_F \right) + l_{1,1}^{(\text{FB})d} \left( \mu_b^2, 0; \eta_b, \eta_F \right) \right\},
\end{aligned} \tag{A1}$$


---

$$\begin{aligned}
\partial_t h_t^2 = & (d - 4 + 2\eta_t + \eta_{\tilde{\phi}}) h_t^2 \\
& - v_d h_t^4 \left\{ l_{1,1}^{(\text{FB})d} \left( \mu_t^2, \mu_G^2; \eta_t, \eta_{\tilde{\phi}} \right) \right. \\
& \left. - l_{1,1}^{(\text{FB})d} \left( \mu_t^2, \mu_H^2; \eta_t, \eta_{\tilde{\phi}} \right) \right\} \\
& - 2v_d h_t^2 h_b^2 l_{1,1}^{(\text{FB})d} \left( \mu_b^2, \mu_G^2; \eta_b, \eta_{\tilde{\phi}} \right) \\
& - 4(3 + \xi) \frac{N_c^2 - 1}{2N_c} g^2 h_t^2 l_{1,1}^{(\text{FB})d} \left( \mu_t^2, 0; \eta_t, \eta_F \right),
\end{aligned} \tag{A2}$$

$$\begin{aligned}
\partial_t h_b^2 = & (d - 4 + 2\eta_b + \eta_{\tilde{\phi}}) h_b^2 \\
& - v_d h_b^4 \left\{ l_{1,1}^{(\text{FB})d} \left( \mu_b^2, \mu_G^2; \eta_b, \eta_{\tilde{\phi}} \right) \right. \\
& \left. - l_{1,1}^{(\text{FB})d} \left( \mu_b^2, \mu_H^2; \eta_b, \eta_{\tilde{\phi}} \right) \right\} \\
& - 2v_d h_b^2 h_t^2 l_{1,1}^{(\text{FB})d} \left( \mu_t^2, \mu_G^2; \eta_t, \eta_{\tilde{\phi}} \right) \\
& - 4(3 + \xi) \frac{N_c^2 - 1}{2N_c} g^2 h_b^2 l_{1,1}^{(\text{FB})d} \left( \mu_b^2, 0; \eta_b, \eta_F \right),
\end{aligned} \tag{A3}$$

where  $\kappa$  denotes the minimum of the scalar potential. Here, we have assumed  $\tilde{h}_t = h_t + h$  and treat  $h_t$  and  $h$  separately, accounting for the rebosonization procedure described above.

Finally, the anomalous dimensions of the bosonic and fermionic fields read

$$\begin{aligned}
\eta_{\phi} = & 2N_c \frac{d\gamma}{d} v_d \left( \tilde{h}_t^2 \left[ m_4^{(\text{F})d} \left( \mu_t^2; \eta_t \right) - \frac{\tilde{h}_t^2}{2} \kappa m_2^{(\text{F})d} \left( \mu_t^2; \eta_t \right) \right] \right. \\
& \left. + \tilde{h}_b^2 \left[ m_4^{(\text{F})d} \left( \mu_b^2; \eta_b \right) - \frac{\tilde{h}_b^2}{2} \kappa m_2^{(\text{F})d} \left( \mu_b^2; \eta_b \right) \right] \right),
\end{aligned} \tag{A4}$$

$$\begin{aligned}
\eta_{\tilde{\phi}} = & 2N_c \frac{d\gamma}{d} v_d h^2 \left( m_4^{(\text{F})d} \left( \mu_t^2; \eta_t \right) + m_4^{(\text{F})d} \left( \mu_b^2; \eta_b \right) \right. \\
& \left. - \frac{h^2}{2} \kappa \left( m_2^{(\text{F})d} \left( \mu_t^2; \eta_t \right) + m_2^{(\text{F})d} \left( \mu_b^2; \eta_b \right) \right) \right),
\end{aligned} \tag{A5}$$

$$\begin{aligned}
\eta_{\text{R}}^t = & 2 \frac{v_d}{d} \tilde{h}_t^2 \left\{ 2m_{1,2}^{(\text{FB})d} \left( \mu_b^2, \mu_G^2; \eta_b, \eta_{\tilde{\phi}} \right) \right. \\
& \left. + m_{1,2}^{(\text{FB})d} \left( \mu_t^2, \mu_G^2; \eta_t, \eta_{\tilde{\phi}} \right) + m_{1,2}^{(\text{FB})d} \left( \mu_t^2, \mu_H^2; \eta_t, \eta_{\tilde{\phi}} \right) \right\} \\
& + v_d h^2 \left\{ 2m_{1,2}^{(\text{FB})d} \left( \mu_b^2, \mu_m^2; \eta_b, \eta_{\tilde{\phi}} \right) \right. \\
& \left. + m_{1,2}^{(\text{FB})d} \left( \mu_t^2, \mu_m^2; \eta_t, \eta_{\tilde{\phi}} \right) + m_{1,2}^{(\text{FB})d} \left( \mu_t^2, \mu_{m,r}^2; \eta_t, \eta_{\tilde{\phi}} \right) \right\},
\end{aligned} \tag{A6}$$

$$\begin{aligned}
\eta_{\text{R}}^b = & 2 \frac{v_d}{d} \tilde{h}_b^2 \left\{ 2m_{1,2}^{(\text{FB})d} \left( \mu_t^2, \mu_G^2; \eta_t, \eta_{\tilde{\phi}} \right) \right. \\
& \left. + m_{1,2}^{(\text{FB})d} \left( \mu_b^2, \mu_G^2; \eta_b, \eta_{\tilde{\phi}} \right) + m_{1,2}^{(\text{FB})d} \left( \mu_b^2, \mu_H^2; \eta_b, \eta_{\tilde{\phi}} \right) \right\} \\
& + v_d h^2 \left\{ 2m_{1,2}^{(\text{FB})d} \left( \mu_t^2, \mu_m^2; \eta_t, \eta_{\tilde{\phi}} \right) \right. \\
& \left. + m_{1,2}^{(\text{FB})d} \left( \mu_b^2, \mu_m^2; \eta_b, \eta_{\tilde{\phi}} \right) + m_{1,2}^{(\text{FB})d} \left( \mu_b^2, \mu_{m,r}^2; \eta_b, \eta_{\tilde{\phi}} \right) \right\},
\end{aligned} \tag{A7}$$

$$\begin{aligned}
\eta_{\text{L}}^t = & 2 \frac{v_d}{d} \tilde{h}_t^2 \left( m_{1,2}^{(\text{FB})d} \left( \mu_t^2, \mu_G^2; \eta_t, \eta_{\tilde{\phi}} \right) \right. \\
& \left. + m_{1,2}^{(\text{FB})d} \left( \mu_t^2, \mu_H^2; \eta_t, \eta_{\tilde{\phi}} \right) \right) \\
& + 2v_d h_b^2 m_{1,2}^{(\text{FB})d} \left( \mu_b^2, \mu_G^2; \eta_b, \eta_{\tilde{\phi}} \right) \\
& + v_d h^2 \left( m_{1,2}^{(\text{FB})d} \left( \mu_t^2, \mu_m^2; \eta_t, \eta_{\tilde{\phi}} \right) \right. \\
& \left. + m_{1,2}^{(\text{FB})d} \left( \mu_t^2, \mu_{m,r}^2; \eta_t, \eta_{\tilde{\phi}} \right) + 2m_{1,2}^{(\text{FB})d} \left( \mu_b^2, \mu_m^2; \eta_b, \eta_{\tilde{\phi}} \right) \right),
\end{aligned} \tag{A8}$$

$$\begin{aligned}
\eta_L^b = & 2 \frac{v_d}{d} \tilde{h}_b^2 \left( m_{1,2}^{(\text{FB})d} (\mu_b^2, \mu_G^2; \eta_b, \eta_\phi) \right. \\
& + m_{1,2}^{(\text{FB})d} (\mu_b^2, \mu_H^2; \eta_b, \eta_\phi) \\
& + 2v_d h_t^2 m_{1,2}^{(\text{FB})d} (\mu_t^2, \mu_G^2; \eta_t, \eta_\phi) \\
& + v_d h^2 \left( m_{1,2}^{(\text{FB})d} (\mu_b^2, \mu_m^2; \eta_b, \eta_{\tilde{\phi}}) \right. \\
& + m_{1,2}^{(\text{FB})d} (\mu_b^2, \mu_{m,r}^2; \eta_b, \eta_{\tilde{\phi}}) \\
& \left. \left. + 2m_{1,2}^{(\text{FB})d} (\mu_t^2, \mu_m^2; \eta_t, \eta_{\tilde{\phi}}) \right) \right).
\end{aligned}$$

Here, it is useful to define anomalous dimensions of the top and bottom quark as

$$\eta^t = \frac{1}{2} (\eta_L^t + \eta_R^t), \quad \eta^b = \frac{1}{2} (\eta_L^b + \eta_R^b). \quad (\text{A9})$$

## Appendix B: Scalar Spectrum

In our quartic approximation, the scalar potential for the different regimes are parametrized as

$$\begin{aligned}
U(\rho, \tilde{\rho}) &= m^2 (\rho + \tilde{\rho}) + \frac{\lambda_1}{2} (\rho + \tilde{\rho})^2 + \lambda_2 \rho \tilde{\rho}, & \text{SYM} \\
U(\rho, \tilde{\rho}) &= \frac{\lambda_1}{2} (\rho + \tilde{\rho} - \kappa)^2 + \lambda_2 \rho \tilde{\rho}, & \text{SSB}
\end{aligned} \quad (\text{B1})$$

where we have used

$$\begin{aligned}
\rho &= \phi^{*a} \phi^a \quad \text{and} \quad \phi = \frac{1}{\sqrt{2}} \begin{pmatrix} \phi_1 + i\phi_2 \\ \phi_4 + i\phi_3 \end{pmatrix}, \\
\tilde{\rho} &= \tilde{\phi}^{*a} \tilde{\phi}^a \quad \text{and} \quad \tilde{\phi} = \frac{1}{\sqrt{2}} \begin{pmatrix} \tilde{\phi}_1 + i\tilde{\phi}_2 \\ \tilde{\phi}_4 + i\tilde{\phi}_3 \end{pmatrix},
\end{aligned} \quad (\text{B2})$$

and the vacuum configuration of the fields are chosen as

$$\phi|_{\text{vac}} = \begin{pmatrix} 0 \\ \sqrt{\kappa} \end{pmatrix}, \quad \tilde{\phi}|_{\text{vac}} = \begin{pmatrix} 0 \\ 0 \end{pmatrix}. \quad (\text{B3})$$

In the symmetric regime we have  $\kappa = 0$ , whereas in the broken regime  $\kappa$  is non-zero.

The mass spectrum of the various components of the two scalar fields (abbreviated by  $f_i$ ) is given by

$$M_{f_i}^2 = \left. \frac{\partial^2 U(\rho, \tilde{\rho})}{\partial f_i^2} \right|_{\text{vac}}. \quad (\text{B4})$$

In the symmetric regime, we find all components of the fields to have the same mass, given by

$$M_{f_i}^2 = m^2. \quad (\text{B5})$$

In the broken regime, the components obtain different masses. The components of the  $\tilde{\phi}$  field acquire a mass

$$M_{\tilde{\phi}_i}^2 = \lambda_2 \kappa. \quad (\text{B6})$$

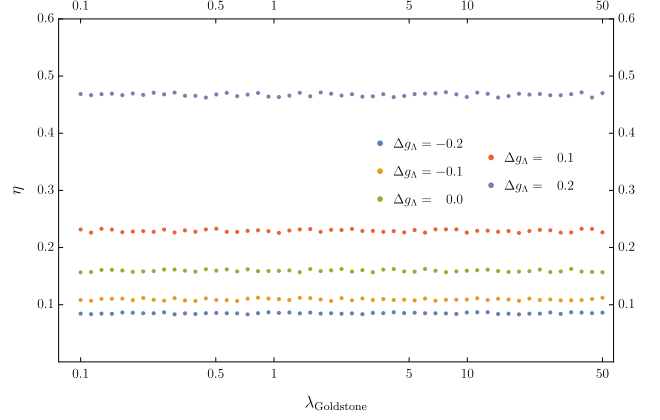


Figure 11. Dependence of the phase transition on the Goldstone mass parameter  $\lambda_{\text{Goldstone}}$ . We find no significant influence on the critical exponent  $\eta$ . This analysis has been performed for a fixed value of  $g_\Lambda = 0.719$ .

For the  $\phi$  field we find

$$\begin{aligned}
M_{\phi_4}^2 &= 2\lambda_1 \kappa \\
M_{\phi_i}^2 &= 0 \quad \text{for } i \neq 4.
\end{aligned} \quad (\text{B7})$$

In comparison to the standard model, these massless Goldstone modes are an artifact of not having included the electroweak gauge sector. The BEH mechanism renders these modes together with the  $W$  and  $Z$  bosons massive. For our purposes, it suffices to model the BEH mechanism by giving a mass to these modes

$$M_{\phi_i}^2 = \lambda_{\text{Goldstone}} \kappa \quad \text{for } i \neq 4 \quad (\text{B8})$$

proportional to the vacuum expectation value. In this way, they are unaffected in the symmetric regime, but decouple in the broken regime. This modeling of the BEH mechanism comes at the expense of a new parameter  $\lambda_{\text{Goldstone}}$ . We study the dependence of the phase transition on this parameter, but find no significant influence on the quantities of interest such as the pseudo-critical exponent, see Fig. 11. For the computational purposes, we simply set this parameter to  $\lambda_{\text{Goldstone}} = 1$  in this work.

It is instructive to compare the scalar spectrum found here for the parametrization (B1) of the potential with that derived from the complete quartic form (11), as discussed in the literature [40]. While the spectrum in the symmetric regime is the same for both potentials, exhibiting 8 degrees of freedom with squared mass  $m^2$ , the masses in the broken regime differ for the two parametrizations. While we have one radial mode with mass  $2\lambda_1 \kappa$  for the SSB potentials in both cases, the full quartic form (11) gives rise to four massless Goldstone modes, and three modes with squared mass  $\lambda_2 \kappa$ , whereas there are only three Goldstone modes and four  $\lambda_2 \kappa$  modes for our potential (B1). The reason for this difference lies in the fact, that the structure of the additional trace invariant  $\tau$  of Eq. (12) is not properly

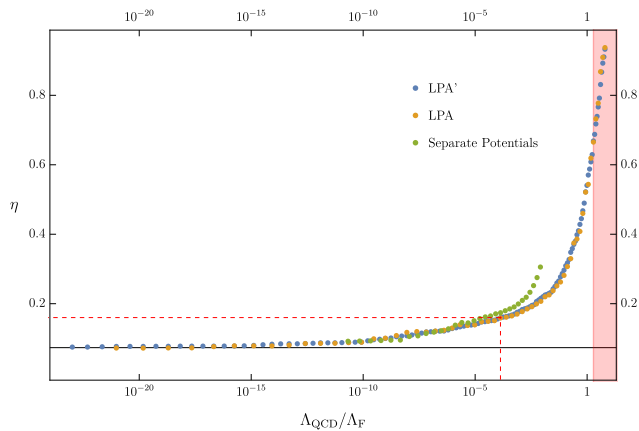


Figure 12. Comparison of the results of this work with the approach used in [44] based on disentangled scalar fields. Despite quantitative differences, we observe qualitative similarities in the sense that an increasingly strong interacting gauge sector alleviates the fine-tuning necessary in the model. The physical point, where the running of the strong gauge coupling coincides with the standard model is denoted by the red dashed line.

taken into account by our parametrization in terms of  $\rho$  and  $\tilde{\rho}$ . Comparing the resulting flow equations for the couplings in the scalar potential shows no difference in the mass parameter  $m^2$  and quartic coupling  $\lambda_1$  beta functions. The difference in the scalar spectrum, however, yields a slightly different flow equation for  $\lambda_2$  as a consequence. To correct for this different parametrization, we use the beta function for the  $\lambda_2$  coupling as it follows from the complete quartic parametrization (11). Nevertheless, we have checked that the use of the beta function that would follow from Eq. (B1) has no significant influence on the results of this work.

### Appendix C: Comparison to an approach with separate scalar fields

In a previous study [44], we have studied the interplay of the chiral transitions using a description where the mesonic degrees of freedom are not combined with the Higgs field into one collective field, but both the meson and Higgs potential are kept separate and disentangled. Whereas two distinct scalar potentials,  $V$  for the mesons and  $U$  for the Higgs field, offer the advantage of straightforwardly identifying the degrees of freedom, it is not as easy to identify the “correct” vacuum.

In the disentangled description, it naively seems possible to have a Higgs potential in the broken regime while the meson potential is still symmetric, or vice versa.

This is, however, modified by the fluctuations, since a non-vanishing vacuum expectation value in one of the potentials induces a linear term in the other potential through the Yukawa interactions, shifting the minimum away from vanishing field amplitude also in the other potential. In the study [44], we have for simplicity assumed that the true vacuum state is given by a linear superposition of the two minima. Subsequently, an analysis analogous to the one in this work is performed. Concentrating on the chiral transitions and the pseudo-critical exponent, we find qualitatively similar results, i.e. the fine-tuning problem gets alleviated for growing gauge couplings in the UV, as is shown in Fig. 12. For more details and computational subtleties, we refer the reader to [44].

### Appendix D: Threshold Functions

The various quantities  $l_n^d(\cdot)$ ,  $m_n^d(\cdot)$ , etc., denote threshold functions. These quantities correspond to loop integrals of the functional renormalization group and parametrize the decoupling of massive modes from the flow equations. These quantities are numerically of order 1, their precise form depends on the regulator. Even though they have been frequently discussed in the literature [8, 40, 56, 70], we list the expressions for the threshold functions used in this work explicitly for completeness.

We define the regularized kinetic terms in momentum space for bosons and fermions as

$$\begin{aligned} P(q) &= q^2 (1 + r_{k,B}(q)), \\ P_F(q) &= q^2 (1 + r_{k,F}(q))^2 \\ &= q^2 (1 + r_{k,L}(q)) (1 + r_{k,R}(q)), \end{aligned}$$

where the last line is used for chiral fermions where regulator shape functions are introduced for the left- and right-handed part, respectively. The general definitions of the threshold functions can be found in the literature [8, 40, 56, 70, 73].

For the present work, we use the piecewise linear regulator [79] for the bosonic regulator shape function

$$r_B = \left( \frac{k^2}{q^2} - 1 \right) \Theta(k^2 - q^2),$$

and define the fermionic one implicitly by

$$(1 + r_B) = (1 + r_L)(1 + r_R), \quad r_L = r_R.$$

This regulator allows to compute the threshold functions analytically which is advantageous for the subsequent numerical integration of the flow equations. The explicit form reads

$$\begin{aligned}
l_n^d(\omega; \eta_\phi) &= \frac{2(\delta_{n,0} + n)}{d} \frac{1 - \frac{\eta_\phi}{d+2}}{(1 + \omega)^{n+1}}, & l_n^{(F)d}(\omega; \eta_\psi) &= \frac{2(\delta_{n,0} + n)}{d} \frac{1 - \frac{\eta_\psi}{d+1}}{(1 + \omega)^{n+1}}, \\
l_{n_1, n_2}^{(FB)d}(\omega_1, \omega_2; \eta_\psi, \eta_\phi) &= \frac{2}{d} \frac{1}{(1 + \omega_1)^{n_1} (1 + \omega_2)^{n_2}} \\
&\quad \left[ \frac{n_1}{1 + \omega_1} \left(1 - \frac{\eta_\psi}{d+1}\right) + \frac{n_2}{1 + \omega_2} \left(1 - \frac{\eta_\phi}{d+2}\right) \right], \\
l_{n_1, n_2, n_3}^{(FBB)d}(\omega_1, \omega_2, \omega_3; \eta_\psi, \eta_{\phi_1}, \eta_{\phi_2}) &= \frac{2}{d} \frac{1}{(1 + \omega_1)^{n_1} (1 + \omega_2)^{n_2} (1 + \omega_3)^{n_3}} \\
&\quad \left[ \frac{n_1}{1 + \omega_1} \left(1 - \frac{\eta_\psi}{d+1}\right) + \frac{n_2}{1 + \omega_2} \left(1 - \frac{\eta_{\phi_1}}{d+2}\right) + \frac{n_3}{1 + \omega_3} \left(1 - \frac{\eta_{\phi_2}}{d+2}\right) \right], \\
m_{n_1, n_2}^d(\omega_1, \omega_2; \eta_\phi) &= \frac{1}{(1 + \omega_1)^{n_1} (1 + \omega_2)^{n_2}}, & m_2^{(F)d}(\omega; \eta_\psi) &= \frac{1}{(1 + \omega)^4}, \\
m_4^{(F)d}(\omega; \eta_\psi) &= \frac{1}{(1 + \omega)^4} + \frac{1 - \eta_\psi}{d-2} \frac{1}{(1 + \omega)^3} - \left( \frac{1 - \eta_\psi}{2d-4} + \frac{1}{4} \right) \frac{1}{(1 + \omega)^2}, \\
m_{n_1, n_2}^{(FB)d}(\omega_1, \omega_2; \eta_\psi, \eta_\phi) &= \left(1 - \frac{\eta_\phi}{d+1}\right) \frac{1}{(1 + \omega_1)^{n_1} (1 + \omega_2)^{n_2}}, \\
\tilde{m}_{1,1}^{(FB)d}(\omega_1, \omega_2; \eta_\psi, \eta_\phi) &= \frac{2}{d-1} \frac{1}{(1 + \omega_1)(1 + \omega_2)} \left( \frac{1 - \frac{\eta_\phi}{d+1}}{1 + \omega_2} + \frac{1 - \frac{\eta_\psi}{d}}{1 + \omega_1} - \frac{1}{2} + \frac{\eta_\psi}{2d} \right).
\end{aligned}$$

## Appendix E: Check of universality violations

Since the ungauged limit of our model, the Higgs-top-bottom model, does not exhibit a UV complete limit, we have to define it with an explicit UV cutoff  $\Lambda$ . This introduces a scheme dependence of our results which can be mapped onto a dependence of the choice of the bare couplings. Still, as long as we study flows which spend a sufficiently long ‘‘RG time’’ near the Gaussian weak-coupling fixed point, the dependence of IR observables on the initial conditions (or on the scheme) becomes suppressed by inverse powers of the cutoff scale  $\Lambda$ . In the case that the limit  $\Lambda \rightarrow \infty$  can be taken, universality violations vanish exactly.

In practice, we need find a compromise between a sufficiently large  $\Lambda$  such that universality violations remain quantitatively irrelevant, and a conveniently small  $\Lambda$  in order to keep the numerical effort manageable. The latter is dominated by the need to ‘‘solve the fine-tuning problem’’ in practice simply by fine-tuning the initial control parameter in order to arrive at a Fermi scale  $v \ll \Lambda$ . For our purposes, the choice  $\Lambda = 10^8$  GeV was turned out to represent such a suitable compromise.

As an example of these universality violations, we show the influence of the marginal Yukawa and scalar self-interaction couplings on the vacuum expectation value  $v$  in the deep QCD regime in Fig. 13. Varying the initial conditions of these couplings at  $\mathcal{O}(1)$ , we observe that the vacuum expectation value  $v$  varies merely on the sub-permille level at most. This illustrates the fact that the IR and the scale of all physical of physical

observables is set only by the gauge coupling.

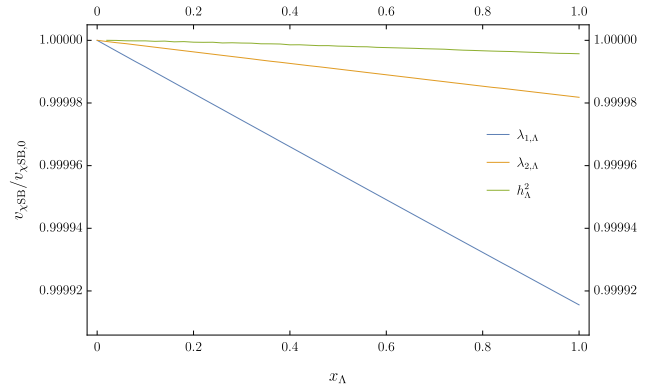


Figure 13. Test of universality violations: normalized vacuum expectation value in the deep QCD regime for different values of the marginal couplings at the UV scale,  $x_\Lambda \in \{\lambda_{1,\Lambda}, \lambda_{2,\Lambda}, h_\Lambda^2\}$  for the lower to upper curve respectively. The initial value of the gauge coupling  $g_\Lambda$  is kept fixed for this analysis. We observe that the vacuum expectation value changes at most on the 0.01% level for changes in the couplings studied in this work.

- [1] Y. Nambu and G. Jona-Lasinio; Dynamical Model of Elementary Particles Based on an Analogy with Superconductivity. 1.; *Phys. Rev.* (1961); **122**:345–358; URL <http://dx.doi.org/10.1103/PhysRev.122.345>.
- [2] S. Weinberg; A Model of Leptons; *Phys. Rev. Lett.* (1967); **19**:1264–1266; URL <http://dx.doi.org/10.1103/PhysRevLett.19.1264>.
- [3] F. Wilczek; Origins of Mass; *Central Eur. J. Phys.* (2012); **10**:1021–1037; URL <http://dx.doi.org/10.2478/s11534-012-0121-0>; 1206.7114.
- [4] S. Durr et al.; Ab-Initio Determination of Light Hadron Masses; *Science* (2008); **322**:1224–1227; URL <http://dx.doi.org/10.1126/science.1163233>; 0906.3599.
- [5] R. L. Workman et al.; Review of Particle Physics; *PTEP* (2022); **2022**:083C01; URL <http://dx.doi.org/10.1093/ptep/ptac097>.
- [6] P. Gerhold and K. Jansen; The Phase structure of a chirally invariant lattice Higgs-Yukawa model for small and for large values of the Yukawa coupling constant; *JHEP* (2007); **09**:041; URL <http://dx.doi.org/10.1088/1126-6708/2007/09/041>; 0705.2539.
- [7] P. Gerhold and K. Jansen; The Phase structure of a chirally invariant lattice Higgs-Yukawa model - numerical simulations; *JHEP* (2007); **10**:001; URL <http://dx.doi.org/10.1088/1126-6708/2007/10/001>; 0707.3849.
- [8] H. Gies and R. Sondenheimer; Higgs Mass Bounds from Renormalization Flow for a Higgs-top-bottom model; *Eur. Phys. J. C* (2015); **75**(2):68; URL <http://dx.doi.org/10.1140/epjc/s10052-015-3284-1>; 1407.8124.
- [9] G. 't Hooft; Naturalness, chiral symmetry, and spontaneous chiral symmetry breaking; *NATO Sci. Ser. B* (1980); **59**:135–157; URL [http://dx.doi.org/10.1007/978-1-4684-7571-5\\_9](http://dx.doi.org/10.1007/978-1-4684-7571-5_9).
- [10] G. F. Giudice; Naturally Speaking: The Naturalness Criterion and Physics at the LHC (2008); 155–178; URL [http://dx.doi.org/10.1142/9789812779762\\_0010](http://dx.doi.org/10.1142/9789812779762_0010); 0801.2562.
- [11] A. Grinbaum; Which fine-tuning arguments are fine?; *Found. Phys.* (2012); **42**:615–631; URL <http://dx.doi.org/10.1007/s10701-012-9629-9>; 0903.4055.
- [12] M. Dine; Naturalness Under Stress; *Ann. Rev. Nucl. Part. Sci.* (2015); **65**:43–62; URL <http://dx.doi.org/10.1146/annurev-nucl-102014-022053>; 1501.01035.
- [13] S. Hossenfelder; Screams for explanation: finetuning and naturalness in the foundations of physics; *Synthese* (2021); **198**(Suppl 16):3727–3745; URL <http://dx.doi.org/10.1007/s11229-019-02377-5>; 1801.02176.
- [14] C. Quigg and R. Shrock; Gedanken Worlds without Higgs: QCD-Induced Electroweak Symmetry Breaking; *Phys. Rev. D* (2009); **79**:096002; URL <http://dx.doi.org/10.1103/PhysRevD.79.096002>; 0901.3958.
- [15] C. Quigg; Unanswered Questions in the Electroweak Theory; *Ann. Rev. Nucl. Part. Sci.* (2009); **59**:505–555; URL <http://dx.doi.org/10.1146/annurev-nucl.010909.083126>; 0905.3187.
- [16] S. Iso, P. D. Serpico and K. Shimada; QCD-Electroweak First-Order Phase Transition in a Supercooled Universe; *Phys. Rev. Lett.* (2017); **119**(14):141301; URL <http://dx.doi.org/10.1103/PhysRevLett.119.141301>; 1704.04955.
- [17] J. Frohlich, G. Morchio and F. Strocchi; Higgs phenomenon without a symmetry breaking order parameter; *Phys. Lett. B* (1980); **97**:249–252; URL [http://dx.doi.org/10.1016/0370-2693\(80\)90594-8](http://dx.doi.org/10.1016/0370-2693(80)90594-8).
- [18] A. Maas; Brout-Englert-Higgs physics: From foundations to phenomenology; *Prog. Part. Nucl. Phys.* (2019); **106**:132–209; URL <http://dx.doi.org/10.1016/j.ppnp.2019.02.003>; 1712.04721.
- [19] A. Maas, R. Sondenheimer and P. Törek; On the observable spectrum of theories with a Brout-Englert-Higgs effect; *Annals Phys.* (2019); **402**:18–44; URL <http://dx.doi.org/10.1016/j.aop.2019.01.010>; 1709.07477.
- [20] R. Sondenheimer; Analytical relations for the bound state spectrum of gauge theories with a Brout-Englert-Higgs mechanism; *Phys. Rev. D* (2020); **101**(5):056006; URL <http://dx.doi.org/10.1103/PhysRevD.101.056006>; 1912.08680.
- [21] A. Maas and R. Sondenheimer; Gauge-invariant description of the Higgs resonance and its phenomenological implications; *Phys. Rev. D* (2020); **102**:113001; URL <http://dx.doi.org/10.1103/PhysRevD.102.113001>; 2009.06671.
- [22] N. Lohitsiri and D. Tong; If the Weak Were Strong and the Strong Were Weak; *SciPost Phys.* (2019); **7**(5):059; URL <http://dx.doi.org/10.21468/SciPostPhys.7.5.059>; 1907.08221.
- [23] J. Berger, A. J. Long and J. Turner; Phase of confined electroweak force in the early Universe; *Phys. Rev. D* (2019); **100**(5):055005; URL <http://dx.doi.org/10.1103/PhysRevD.100.055005>; 1906.05157.
- [24] J. S. Schwinger; A Theory of the Fundamental Interactions; *Annals Phys.* (1957); **2**:407–434; URL [http://dx.doi.org/10.1016/0003-4916\(57\)90015-5](http://dx.doi.org/10.1016/0003-4916(57)90015-5).
- [25] M. Gell-Mann and M. Levy; The axial vector current in beta decay; *Nuovo Cim.* (1960); **16**:705; URL <http://dx.doi.org/10.1007/BF02859738>.
- [26] D. U. Jungnickel and C. Wetterich; Effective action for the chiral quark-meson model; *Phys. Rev. D* (1996); **53**:5142–5175; URL <http://dx.doi.org/10.1103/PhysRevD.53.5142>; hep-ph/9505267.
- [27] B.-J. Schaefer and H.-J. Pirner; Renormalization group flow and equation of state of quarks and mesons; *Nucl. Phys. A* (1999); **660**:439–474; URL [http://dx.doi.org/10.1016/S0375-9474\(99\)00409-1](http://dx.doi.org/10.1016/S0375-9474(99)00409-1); nucl-th/9903003.
- [28] J. Braun, K. Schwenzer and H.-J. Pirner; Linking the quark meson model with QCD at high temperature; *Phys. Rev. D* (2004); **70**:085016; URL <http://dx.doi.org/10.1103/PhysRevD.70.085016>; hep-ph/0312277.
- [29] S. Resch, F. Rennecke and B.-J. Schaefer; Mass sensitivity of the three-flavor chiral phase transition; *Phys. Rev. D* (2019); **99**(7):076005; URL <http://dx.doi.org/10.1103/PhysRevD.99.076005>; 1712.07961.
- [30] J. Eser, F. Divotgey, M. Mitter and D. H. Rischke; Low-energy limit of the  $O(4)$  quark-meson model from the functional renormalization group approach; *Phys. Rev. D* (2018); **98**(1):014024; URL <http://dx.doi.org/10.1103/PhysRevD.98.014024>; 1804.01787.
- [31] F. Divotgey, J. Eser and M. Mitter; Dynamical generation of low-energy couplings from quark-meson

- fluctuations; *Phys. Rev. D* (2019); **99**(5):054023; URL <http://dx.doi.org/10.1103/PhysRevD.99.054023>; 1901.02472.
- [32] J. Braun, M. Leonhardt and M. Pospiech; Fierz-complete NJL model study III: Emergence from quark-gluon dynamics; *Phys. Rev. D* (2020); **101**(3):036004; URL <http://dx.doi.org/10.1103/PhysRevD.101.036004>; 1909.06298.
- [33] D. J. Gross and F. Wilczek; Ultraviolet Behavior of Non-Abelian Gauge Theories; *Phys. Rev. Lett.* (1973); **30**:1343–1346; URL <http://dx.doi.org/10.1103/PhysRevLett.30.1343>.
- [34] H. D. Politzer; Reliable Perturbative Results for Strong Interactions?; *Phys. Rev. Lett.* (1973); **30**:1346–1349; URL <http://dx.doi.org/10.1103/PhysRevLett.30.1346>.
- [35] J. M. Pawłowski; Exact flow equations and the  $U(1)$  problem; *Phys. Rev. D* (1998); **58**:045011; URL <http://dx.doi.org/10.1103/PhysRevD.58.045011>; hep-th/9605037.
- [36] H. Gies, J. Jaeckel, J. M. Pawłowski and C. Wetterich; Do instantons like a colorful background?; *Eur. Phys. J. C* (2007); **49**:997–1010; URL <http://dx.doi.org/10.1140/epjc/s10052-006-0178-2>; hep-ph/0608171.
- [37] R. D. Pisarski and F. Rennecke; Multi-instanton contributions to anomalous quark interactions; *Phys. Rev. D* (2020); **101**(11):114019; URL <http://dx.doi.org/10.1103/PhysRevD.101.114019>; 1910.14052.
- [38] G. Fejős; Perturbative RG analysis of the condensate dependence of the axial anomaly in the three flavor linear sigma model; *Symmetry* (2021); **13**(3):488; URL <http://dx.doi.org/10.3390/sym13030488>; 2012.08706.
- [39] J. Braun, M. Leonhardt, J. M. Pawłowski and D. Rosenblüh; Chiral and effective  $U(1)_A$  symmetry restoration in QCD (2020); 2012.06231.
- [40] D. Jungnickel and C. Wetterich; Effective action for the chiral quark-meson model; *Phys. Rev. D* (1996); **53**:5142–5175; URL <http://dx.doi.org/10.1103/PhysRevD.53.5142>; hep-ph/9505267.
- [41] S. Schreyer; Global stability of scalar potentials in asymptotically safe particle models (2020); URL <https://nbn-resolving.org/urn:nbn:de:gbv:27-dbt-20201006-093946-005>.
- [42] N. A. Tornqvist; Mixing the strong and E-W Higgs sectors; *Phys. Lett. B* (2005); **619**:145–148; URL <http://dx.doi.org/10.1016/j.physletb.2005.05.058>; hep-ph/0504204.
- [43] M. Schumacher; Structure of Scalar Mesons and the Higgs Sector of Strong Interaction; *J. Phys. G* (2011); **38**:083001; URL <http://dx.doi.org/10.1088/0954-3899/38/8/083001>; 1106.1015.
- [44] R. Schmieden; Aspects of the Gauge Hierarchy of the Standard Model; *Master Thesis* (2020); Jena; URL <http://dx.doi.org/10.22032/dbt.47615>.
- [45] V. A. Miransky, M. Tanabashi and K. Yamawaki; Dynamical Electroweak Symmetry Breaking with Large Anomalous Dimension and  $t$  Quark Condensate; *Phys. Lett. B* (1989); **221**:177–183; URL [http://dx.doi.org/10.1016/0370-2693\(89\)91494-9](http://dx.doi.org/10.1016/0370-2693(89)91494-9).
- [46] V. A. Miransky, M. Tanabashi and K. Yamawaki; Is the  $t$  Quark Responsible for the Mass of  $W$  and  $Z$  Bosons?; *Mod. Phys. Lett. A* (1989); **4**:1043; URL <http://dx.doi.org/10.1142/S0217732389001210>.
- [47] W. A. Bardeen, C. T. Hill and M. Lindner; Minimal Dynamical Symmetry Breaking of the Standard Model; *Phys. Rev. D* (1990); **41**:1647; URL <http://dx.doi.org/10.1103/PhysRevD.41.1647>.
- [48] C. T. Hill and E. H. Simmons; Strong Dynamics and Electroweak Symmetry Breaking; *Phys. Rept.* (2003); **381**:235–402; URL [http://dx.doi.org/10.1016/S0370-1573\(03\)00140-6](http://dx.doi.org/10.1016/S0370-1573(03)00140-6); [Erratum: *Phys.Rept.* 390, 553–554 (2004)]; hep-ph/0203079.
- [49] L. von Smekal, R. Alkofer and A. Hauck; The Infrared behavior of gluon and ghost propagators in Landau gauge QCD; *Phys. Rev. Lett.* (1997); **79**:3591–3594; URL <http://dx.doi.org/10.1103/PhysRevLett.79.3591>; hep-ph/9705242.
- [50] H. Gies; Running coupling in Yang-Mills theory: A flow equation study; *Phys. Rev. D* (2002); **66**:025006; URL <http://dx.doi.org/10.1103/PhysRevD.66.025006>; hep-th/0202207.
- [51] C. S. Fischer and R. Alkofer; Nonperturbative propagators, running coupling and dynamical quark mass of Landau gauge QCD; *Phys. Rev. D* (2003); **67**:094020; URL <http://dx.doi.org/10.1103/PhysRevD.67.094020>; hep-ph/0301094.
- [52] J. M. Pawłowski, D. F. Litim, S. Nedelko and L. von Smekal; Infrared behavior and fixed points in Landau gauge QCD; *Phys. Rev. Lett.* (2004); **93**:152002; URL <http://dx.doi.org/10.1103/PhysRevLett.93.152002>; hep-th/0312324.
- [53] C. S. Fischer, A. Maas and J. M. Pawłowski; On the infrared behavior of Landau gauge Yang-Mills theory; *Annals Phys.* (2009); **324**:2408–2437; URL <http://dx.doi.org/10.1016/j.aop.2009.07.009>; 0810.1987.
- [54] A. Weber; Epsilon Expansion for Infrared Yang-Mills theory in Landau Gauge; *Phys. Rev. D* (2012); **85**:125005; URL <http://dx.doi.org/10.1103/PhysRevD.85.125005>; 1112.1157.
- [55] U. Reinosa, J. Serreau, M. Tissier and N. Wschebor; How nonperturbative is the infrared regime of Landau gauge Yang-Mills correlators?; *Phys. Rev. D* (2017); **96**(1):014005; URL <http://dx.doi.org/10.1103/PhysRevD.96.014005>; 1703.04041.
- [56] H. Gies and C. Wetterich; Universality of spontaneous chiral symmetry breaking in gauge theories; *Physical Review D* (2004); **69**(2); URL <http://dx.doi.org/10.1103/PhysRevD.69.025001>; hep-th/0209183.
- [57] V. A. Miransky; Dynamics of Spontaneous Chiral Symmetry Breaking and Continuum Limit in Quantum Electrodynamics; *Nuovo Cim. A* (1985); **90**:149–170; URL <http://dx.doi.org/10.1007/BF02724229>.
- [58] H. Gies and J. Jaeckel; Chiral phase structure of QCD with many flavors; *Eur. Phys. J. C* (2006); **46**:433–438; URL <http://dx.doi.org/10.1140/epjc/s2006-02475-0>; hep-ph/0507171.
- [59] J. Braun and H. Gies; Chiral phase boundary of QCD at finite temperature; *JHEP* (2006); **06**:024; URL <http://dx.doi.org/10.1088/1126-6708/2006/06/024>; hep-ph/0602226.
- [60] J. Braun, C. S. Fischer and H. Gies; Beyond Miransky Scaling; *Phys. Rev. D* (2011); **84**:034045; URL <http://dx.doi.org/10.1103/PhysRevD.84.034045>; 1012.4279.
- [61] M. Mitter, J. M. Pawłowski and N. Strodthoff; Chiral symmetry breaking in continuum QCD; *Phys. Rev. D* (2015); **91**:054035; URL <http://dx.doi.org/10.1103/PhysRevD.91.054035>; 1503.03401.

- 1103/PhysRevD.91.054035; 1411.7978.
- [62] J. Braun, L. Fister, J. M. Pawłowski and F. Rennecke; From Quarks and Gluons to Hadrons: Chiral Symmetry Breaking in Dynamical QCD; Phys. Rev. D (2016); **94**(3):034016; URL <http://dx.doi.org/10.1103/PhysRevD.94.034016>; 1412.1045.
- [63] G. Eichmann, H. Sanchis-Alepuz, R. Williams, R. Alkofer and C. S. Fischer; Baryons as relativistic three-quark bound states; Prog. Part. Nucl. Phys. (2016); **91**:1–100; URL <http://dx.doi.org/10.1016/j.ppnp.2016.07.001>; 1606.09602.
- [64] D. Binosi, L. Chang, J. Papavassiliou, S.-X. Qin and C. D. Roberts; Natural constraints on the gluon-quark vertex; Phys. Rev. D (2017); **95**(3):031501; URL <http://dx.doi.org/10.1103/PhysRevD.95.031501>; 1609.02568.
- [65] A. K. Cyrol, M. Mitter, J. M. Pawłowski and N. Strodthoff; Nonperturbative quark, gluon, and meson correlators of unquenched QCD; Phys. Rev. D (2018); **97**(5):054006; URL <http://dx.doi.org/10.1103/PhysRevD.97.054006>; 1706.06326.
- [66] C. Wetterich; Exact evolution equation for the effective potential; Phys. Lett. B (1993); **301**:90–94; URL [http://dx.doi.org/10.1016/0370-2693\(93\)90726-X](http://dx.doi.org/10.1016/0370-2693(93)90726-X); 1710.05815.
- [67] U. Ellwanger; FLOW equations for N point functions and bound states; Z. Phys. C (1994); **62**:503–510; URL <http://dx.doi.org/10.1007/BF01555911>; hep-ph/9308260.
- [68] T. R. Morris; The Exact renormalization group and approximate solutions; Int. J. Mod. Phys. A (1994); **9**:2411–2450; URL <http://dx.doi.org/10.1142/S0217751X94000972>; hep-ph/9308265.
- [69] M. Bonini, M. D’Attanasio and G. Marchesini; Perturbative renormalization and infrared finiteness in the Wilson renormalization group: The Massless scalar case; Nucl. Phys. B (1993); **409**:441–464; URL [http://dx.doi.org/10.1016/0550-3213\(93\)90588-G](http://dx.doi.org/10.1016/0550-3213(93)90588-G); hep-th/9301114.
- [70] J. Berges, N. Tetradis and C. Wetterich; Non-perturbative renormalization flow in quantum field theory and statistical physics; Physics Reports (2002); **363**(4-6):223–386; URL [http://dx.doi.org/10.1016/S0370-1573\(01\)00098-9](http://dx.doi.org/10.1016/S0370-1573(01)00098-9).
- [71] H. Gies; Introduction to the functional RG and applications to gauge theories; Lect. Notes Phys. (2012); **852**:287–348; URL [http://dx.doi.org/10.1007/978-3-642-27320-9\\_6](http://dx.doi.org/10.1007/978-3-642-27320-9_6); hep-ph/0611146.
- [72] J. M. Pawłowski; Aspects of the functional renormalisation group; Annals Phys. (2007); **322**:2831–2915; URL <http://dx.doi.org/10.1016/j.aop.2007.01.007>; hep-th/0512261.
- [73] J. Braun; Fermion Interactions and Universal Behavior in Strongly Interacting Theories; J. Phys. G (2012); **39**:033001; URL <http://dx.doi.org/10.1088/0954-3899/39/3/033001>; 1108.4449.
- [74] P. Kopietz, L. Bartosch and F. Schütz; Introduction to the functional renormalization group; vol. 798 (2010); URL <http://dx.doi.org/10.1007/978-3-642-05094-7>.
- [75] N. Dupuis, L. Canet, A. Eichhorn, W. Metzner, J. M. Pawłowski, M. Tissier and N. Wschebor; The nonperturbative functional renormalization group and its applications; Phys. Rept. (2021); **910**:1–114; URL <http://dx.doi.org/10.1016/j.physrep.2021.01.001>; 2006.04853.
- [76] W. E. Caswell and F. Wilczek; On the Gauge Dependence of Renormalization Group Parameters; Phys. Lett. B (1974); **49**:291–292; URL [http://dx.doi.org/10.1016/0370-2693\(74\)90437-7](http://dx.doi.org/10.1016/0370-2693(74)90437-7).
- [77] U. Ellwanger, M. Hirsch and A. Weber; Flow equations for the relevant part of the pure Yang-Mills action; Z. Phys. C (1996); **69**:687–698; URL <http://dx.doi.org/10.1007/s002880050073>; hep-th/9506019.
- [78] D. F. Litim and J. M. Pawłowski; Flow equations for Yang-Mills theories in general axial gauges; Physics Letters B (1998); **435**(1-2):181–188; URL [http://dx.doi.org/10.1016/S0370-2693\(98\)00761-8](http://dx.doi.org/10.1016/S0370-2693(98)00761-8).
- [79] D. F. Litim; Optimized renormalization group flows; Physical Review D (2001); **64**(10); URL <http://dx.doi.org/10.1103/physrevd.64.105007>.
- [80] J. Borchardt and A. Eichhorn; Universal behavior of coupled order parameters below three dimensions; Phys. Rev. E (2016); **94**(4):042105; URL <http://dx.doi.org/10.1103/PhysRevE.94.042105>; 1606.07449.
- [81] A. J. Beekman and G. Fejős; Charged and neutral fixed points in the  $O(N) \oplus O(N)$ -model with Abelian gauge fields; Phys. Rev. D (2019); **100**(1):016005; URL <http://dx.doi.org/10.1103/PhysRevD.100.016005>; 1903.05331.
- [82] H. Gies and C. Wetterich; Renormalization flow of bound states; Phys. Rev. D (2002); **65**:065001; URL <http://dx.doi.org/10.1103/PhysRevD.65.065001>; hep-th/0107221.
- [83] H. Gies and C. Wetterich; Renormalization flow from UV to IR degrees of freedom; Acta Phys. Slov. (2002); **52**(4):215–220; hep-ph/0205226.
- [84] S. Floerchinger and C. Wetterich; Exact flow equation for composite operators; Phys. Lett. B (2009); **680**:371–376; URL <http://dx.doi.org/10.1016/j.physletb.2009.09.014>; 0905.0915.
- [85] A. Baldazzi, R. B. A. Zinati and K. Falls; Essential renormalisation group; SciPost Phys. (2022); **13**(4):085; URL <http://dx.doi.org/10.21468/SciPostPhys.13.4.085>; 2105.11482.
- [86] F. Ihssen and J. M. Pawłowski; Flowing fields and optimal RG-flows (2023); 2305.00816.
- [87] H. Gies, J. Jaeckel and C. Wetterich; Towards a renormalizable standard model without fundamental Higgs scalar; Phys. Rev. D (2004); **69**:105008; URL <http://dx.doi.org/10.1103/PhysRevD.69.105008>; hep-ph/0312034.
- [88] J. Zinn-Justin; Quantum field theory and critical phenomena; Int. Ser. Monogr. Phys. (2002); **113**:1–1054.
- [89] B. Pendleton and G. G. Ross; Mass and Mixing Angle Predictions from Infrared Fixed Points; Phys. Lett. B (1981); **98**:291–294; URL [http://dx.doi.org/10.1016/0370-2693\(81\)90017-4](http://dx.doi.org/10.1016/0370-2693(81)90017-4).
- [90] N.-P. Chang; Eigenvalue conditions and asymptotic freedom for Higgs-scalar gauge theories; Phys. Rev. D (1974); **10**:2706–2709; URL <http://dx.doi.org/10.1103/PhysRevD.10.2706>.
- [91] D. J. E. Callaway; Triviality Pursuit: Can Elementary Scalar Particles Exist?; Phys. Rept. (1988); **167**:241; URL [http://dx.doi.org/10.1016/0370-1573\(88\)90008-7](http://dx.doi.org/10.1016/0370-1573(88)90008-7).
- [92] W. Zimmermann; Reduction in the Number of Coupling Parameters; Commun. Math. Phys.

- (1985); **97**:211; URL <http://dx.doi.org/10.1007/BF01206187>.
- [93] S. Heinemeyer, J. Kubo, M. Mondragon, O. Piguet, K. Sibold, W. Zimmermann and G. Zoupanos; Reduction of couplings and its application in particle physics, Finite theories, Higgs and top mass predictions; PoS (2014); **Higgs and top**:1–339; 1411.7155.
- [94] A. D. Bond and D. F. Litim; Theorems for Asymptotic Safety of Gauge Theories; Eur. Phys. J. C (2017); **77**(6):429; URL <http://dx.doi.org/10.1140/epjc/s10052-017-4976-5>; [Erratum: Eur.Phys.J.C 77, 525 (2017)]; 1608.00519.
- [95] G. F. Giudice, G. Isidori, A. Salvio and A. Strumia; Softened Gravity and the Extension of the Standard Model up to Infinite Energy; JHEP (2015); **02**:137; URL [http://dx.doi.org/10.1007/JHEP02\(2015\)137](http://dx.doi.org/10.1007/JHEP02(2015)137); 1412.2769.
- [96] H. Gies and L. Zambelli; Asymptotically free scaling solutions in non-Abelian Higgs models; Phys. Rev. D (2015); **92**(2):025016; URL <http://dx.doi.org/10.1103/PhysRevD.92.025016>; 1502.05907.
- [97] H. Gies and L. Zambelli; Non-Abelian Higgs models: Paving the way for asymptotic freedom; Phys. Rev. D (2017); **96**(2):025003; URL <http://dx.doi.org/10.1103/PhysRevD.96.025003>; 1611.09147.
- [98] T. P. Cheng, E. Eichten and L.-F. Li; Higgs Phenomena in Asymptotically Free Gauge Theories; Phys. Rev. D (1974); **9**:2259; URL <http://dx.doi.org/10.1103/PhysRevD.9.2259>.
- [99] H. Gies, R. Sondenheimer, A. Ugoletti and L. Zambelli; Asymptotic freedom in  $\mathbb{Z}_2$ -Yukawa-QCD models; The European Physical Journal C (2019); **79**(2); URL <http://dx.doi.org/10.1140/epjc/s10052-019-6604-z>.
- [100] H. Gies, R. Sondenheimer, A. Ugoletti and L. Zambelli; Scheme Dependence of Asymptotically Free Solutions; The European Physical Journal C (2019); **79**(6); URL <http://dx.doi.org/10.1140/epjc/s10052-019-6956-4>.